ISSN 0736-5306

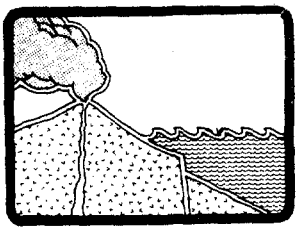

SCIENCE OF TSUNAMI HAZARDS

The International Journal of The Tsunami Society

Volume 4 Number 3 1986

OBJECTIVE: The Tsunami Society publishes this journal to increase and disseminate knowledge about tsunamis and their hazards.

DISCLAIMER: The Tsunami Society publishes this journal to disseminate information relating to tsunamis. Although these articles have been technically reviewed by peers, The Tsunami Society is not responsible for the variety of any statement, opinion, or consequences.

EDITOR'S NOTE

The Tsunami Society is now four years old. The society wishes to introduce new items in addition to those in the Tsunami Dialogue, of which the first issue has already been published. This journal will now include a new section entitled "Forum" which will involve brief discussions on technical matters related to tsunamis and comments on articles that appeared in any issue, up to one year ago. Please note that papers submitted to the Forum must be limited to four typed pages, double-spaced. If your discussion must be longer in length it should be submitted as a paper on its own merit. Non-technical items may be published in Dialog.

Submit manuscripts of articles, notes, or letters to:

T. S. Murty Technical Editor
Institute of Ocean Sciences
Department of Fisheries and Oceans
Sidney, B.C., Canada V8L 4B2

If article is accepted for publication the author(s) must submit a camera ready manuscript. A voluntary $50.00 page charge will include 50 reprints.

SUBSCRIPTION INFORMATION: Price per copy $20.00 USA

ISSN 0736-5306

Published by **The Tsunami Society** in Honolulu, Hawaii, U.S.A.

TSUNAMIGENIC EARTHQUAKES IN CHINA: 1831 B.C. to 1980 A.D

Zhou Qinghai* and William M. Adams**

ABSTRACT

Four thousand one hundred seventeen (4,117) earthquakes of magnitude greater than four and three quarters (4 3/4) have been historically documented as occurring in China for the time period 1831 B.C. to 1980. Of these, only fifteen are certainly or probably tsunamigenic, dating from 47 B.C. to 1921. Based on additional descriptive texts, three events have been evaluated as being storm surges which occurred concurrently with the tsunamis. This study presents the historical data for the tsunamigenic earthquakes in China in relation to the geological and geophysical characteristics of three prominant seismic zones for China, the Eastern seismic zone, the Western seismic zone, and the Taiwan seismic zone. These historical data provide the basis for the development of zonation maps of tsunami hazard for the coastal areas of China.

* National Marine Environmental Forecasting Center, Beijing, PRC
** Hawaii Institute of Geophysics, University of Hawaii, Honolulu, Hawaii, USA

I. INTRODUCTION

China is a country of large geographical area and a lengthy oceanic coastline. The coastline (Figure 1) extends for 1800 km, from the north, at the boundary of China and Korea to the south at the boundary of China and Vietnam. Ten provinces form the border of China (see Figure 1). The area along the coastline of China is well suited to farming and the development of industry. The China coast has many good bays and harbors, some of which are characterized by steep cliffs and deep water. Oceangoing ships enter the ports in connection with transportation, commerce, fishery, and the marine chemicals industry. For these reasons the coastal areas of China are especially vulnerable to the hazards of tsunami impact and inundation.

II. Oceanographic and Geologic Setting of China

1. Oceanography

Offshore in the China Sea, the continental shelf is broad, and the water is shallow. Water depth along the coastline of Zhejiang and Fujian provinces is about 40 meters or less. The average depth is a few tens of meters in the Bohai Sea and Yellow Sea, and the deepest water is only about 100 meters. From the mouth of the Yangtze River down to the south into the East China Sea, the water depth increases to an average of about 300 meters. In the South China Sea, where the water is the deepest in the China region--5,400 meters--the average is more than 1,000 meters. Offshore exploration for mineral resources is being conducted in many areas of the China Sea.

The tidal fluctuations along the China coast approach from the Pacific Ocean and are dominantly diurnal and semidiurnal. In the East China Sea, the tide consists of progressive waves, whereas in the Bohai Sea and Yellow Sea, it appears as rotative waves. In the middle part of the South China Sea, the tidal energy is in the form of progressive waves, but in the coves of this area it occurs as rotative waves. The tide range in the China Sea overall is about 3 meters. The range is greatest along the coastline of Zhejiang and northern Fujian provinces. The spring-tide range at the Fujian coast is 5.7 meters, and the spring-tide range near Hangzhou is 8.0 meters.

2. Seismicity of China

China is a country of abundant earthquakes that are related to the interaction of the Asia-Europe, Pacific, and Indian Ocean plates. See figure 2. The changes in China's geological structure are closely related to these three plates. Before the Palaeozoic Era, the geological activity of China was mainly controlled by the Asia-Europe plate. In the middle of the Cenozoic Era, the activity was affected by interactions of the Pacific and Indian Ocean plates. Most of the present-day earthquakes in China are generated in the area of plate-connecting belts within the continent where severe geological change takes place.

The earthquakes generated in China are commonly distributed in seismic belts. Three seismic zones can be described according to seismological characteristics.

(1) Eastern earthquake zone. This zone is mainly located in the coastal provinces and Shanxi. In this zone, the seismic activity is characterized by high intensity and a long recurrence time.

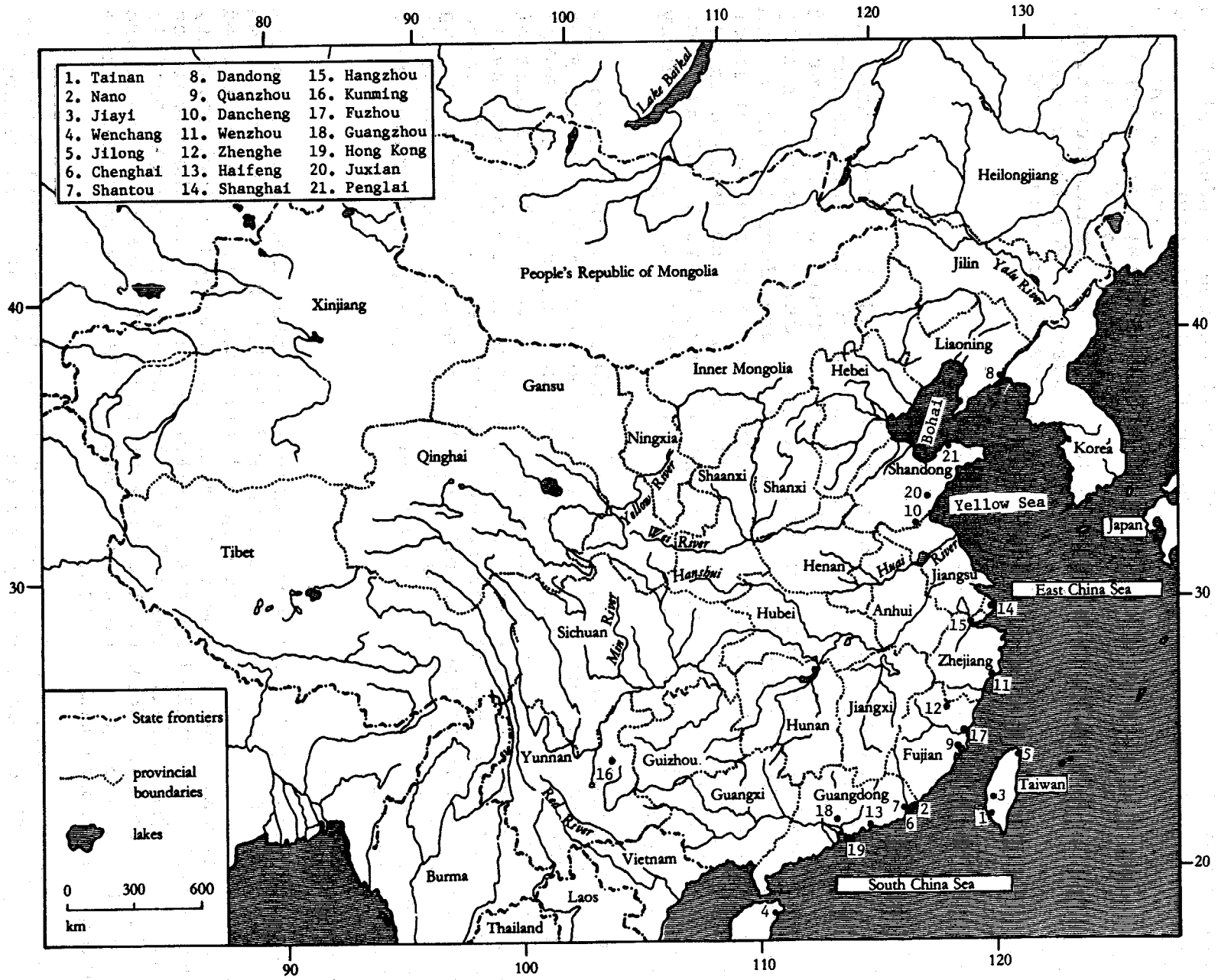

Figure 1: Outline map showing location of provinces in China and of other places mentioned in the text.

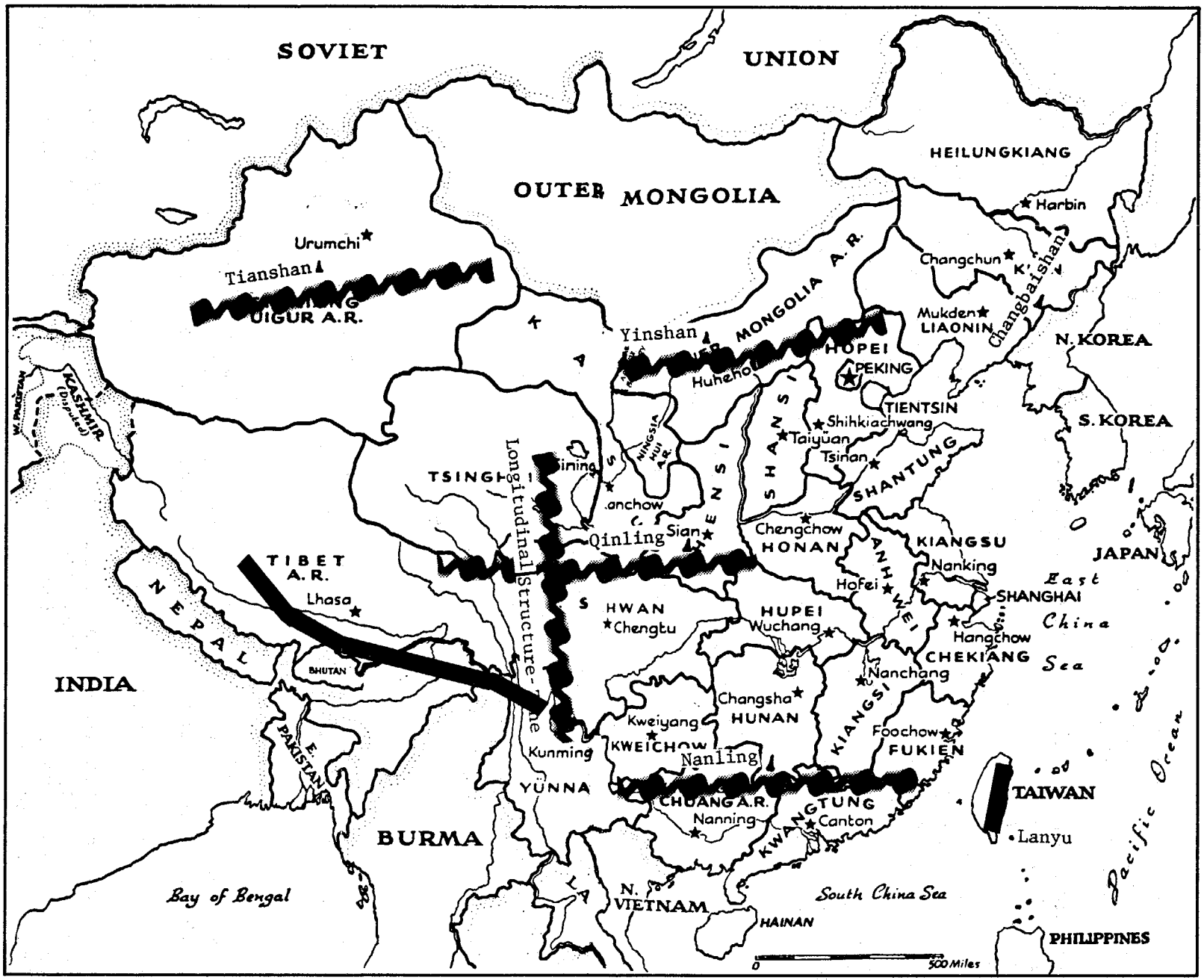

Figure 2: Outline map showing location and orientation of some of the principle tectonic zones of China. The solid lines show the margins of the Asian plate.

(2) Western earthquake zone. This zone is mainly located in Xinjiang, Tibet, and other western provinces. Earthquakes have been found to occur more often in the western part of China than in the eastern part. The western zone is characterized by earthquakes of high frequency as well as high intensity.

(3) Taiwan earthquake zone. Taiwan is the zone having the highest frequency of earthquakes. This zone is characterized by earthquakes with high intensity and a short recurrence time.

Earthquakes in China have shallow, intermediate, and deep focal depths. Shallow focal depth earthquakes have the broadest spatial distribution. Of these the focal depths are at less than 60 km in Taiwan (Figure 3), (and see Figure 2, also), less than 20 km in south China, and between 5-30 km in the north. In general, the foci of shallow focal-depth earthquakes in eastern China are less than 30 km, whereas in western China they are somewhat deeper--about 50-60 km. Middle-depth earthquakes are mainly generated in two areas: the Pamier region along the western boundary of China, where the depth is about 100-160 km; and the northeastern part of Taiwan and its southeast basin area, where the maximum depth is about 270 km. Deep-focus earthquakes are found only in Jilin province where the greatest depth is 590 km.

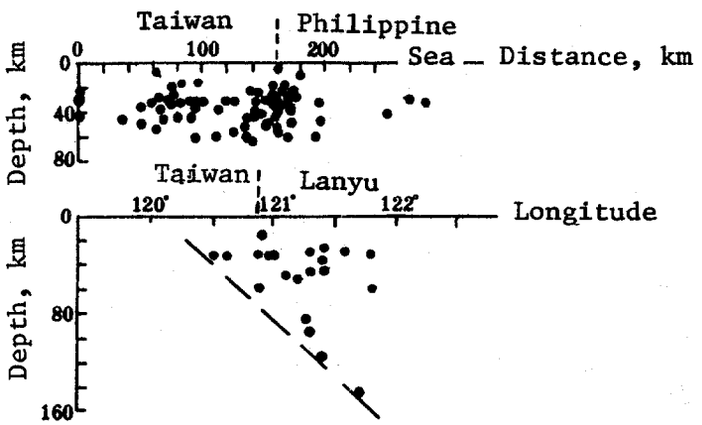

Figure 3: Cross-section plot of the foci of 92 earthquakes. The sections run offshore from Taiwan and range from 119.5 to 123 degrees longitude.

Earthquake activity is closely related to geological structure. In China, the geological structures can be classified into several systems as follows (P. F. Fan, 1986a, 1986b; Li, 1980; Zhang et al., 1984):

(1) Latitudinal Structure System:

This system parallels the latitudes and has a long and complicated history of activity. In China, there are three large, active latitudinal structure zones: the zones of the Tianshan-Yinshan, Qinling, and Nanling mountains. See Figure 2.

(2) Longitudinal Structure System:

The largest longitudinal structure zone, stretching from the western part of Sichuan province to Kunming at Yunnan, consists mainly of a series

of fold belts and two large faults, as well as the structure belt of the western part of Yunnan province. It has a long history of activity, mainly wrench-faulting, that dominates the changes to the geosynclines of the Pliocene and Pleistocene.

(3) Xinhuaxia Structure System:

This young structure system consists of a few uplifting and sinking belts extending in a northeasterly direction: it is at the eastern part of the Asia continental plate. As a result of intense interaction with the latitudinal structure system, some structures have been formed in the shape of a reversed "S".

(4) Qilu Helan Shanzixing Structure System:

This large structure system crosses the northwest and southern parts of China and consists of a series of folds, and overthrust and wrench faults. The eastern part of the system is affected intensely by the Xinhuaxia system; its western part, however, is affected by both the Longxi and Hexi systems.

Other structure systems are the Hexi system, the Longxi system, and the system of the Himalayas Arc.

3. Potential Fields

The seismic activity in China is related to deep crustal structure and therefore the various potential fields.

In China, Bouguer gravity anomalies decrease gradually from east to west. The Bouguer gravity anomalies are about 10 milligals at the southeast coast, but become -500 milligals at Gansu and southern Tibet province, as shown in Figure 4 (National Bureau of Seismology, page 69, 1981). Several broad belts of gravity anomalies trend northeast, north-northeast, approximately north to south, northwest, and approximately east to west. These belts are as follows:

(1) the southeast coastal belt, paralleling the southeast coastline of China,

(2) the Changbai Shan belt, extending from the Changbai Shan pass near Korea to the Bohai Sea; and

(3) the Longmenshan belt, which originates from the south side of Qinling (see Figure 2) and extends in a northeast direction.

Other belts are the Taiwan belt and the Nanling belt.

III. TSUNAMIGENIC EARTHQUAKES

In Chinese history, over the past 3,000 years or so, earthquake events and facts were recorded in classical and folk literature. Scientists of the Peoples' Republic of China have completed an extensive analysis and evaluation of these various data and compiled the results in several recent publications (Gu Gongxu et al., 1983; Xie Yushou and Cai Meipiao, 1983). For the first time, an extensive historical data base on China earthquakes in China has been made available to the international research community.

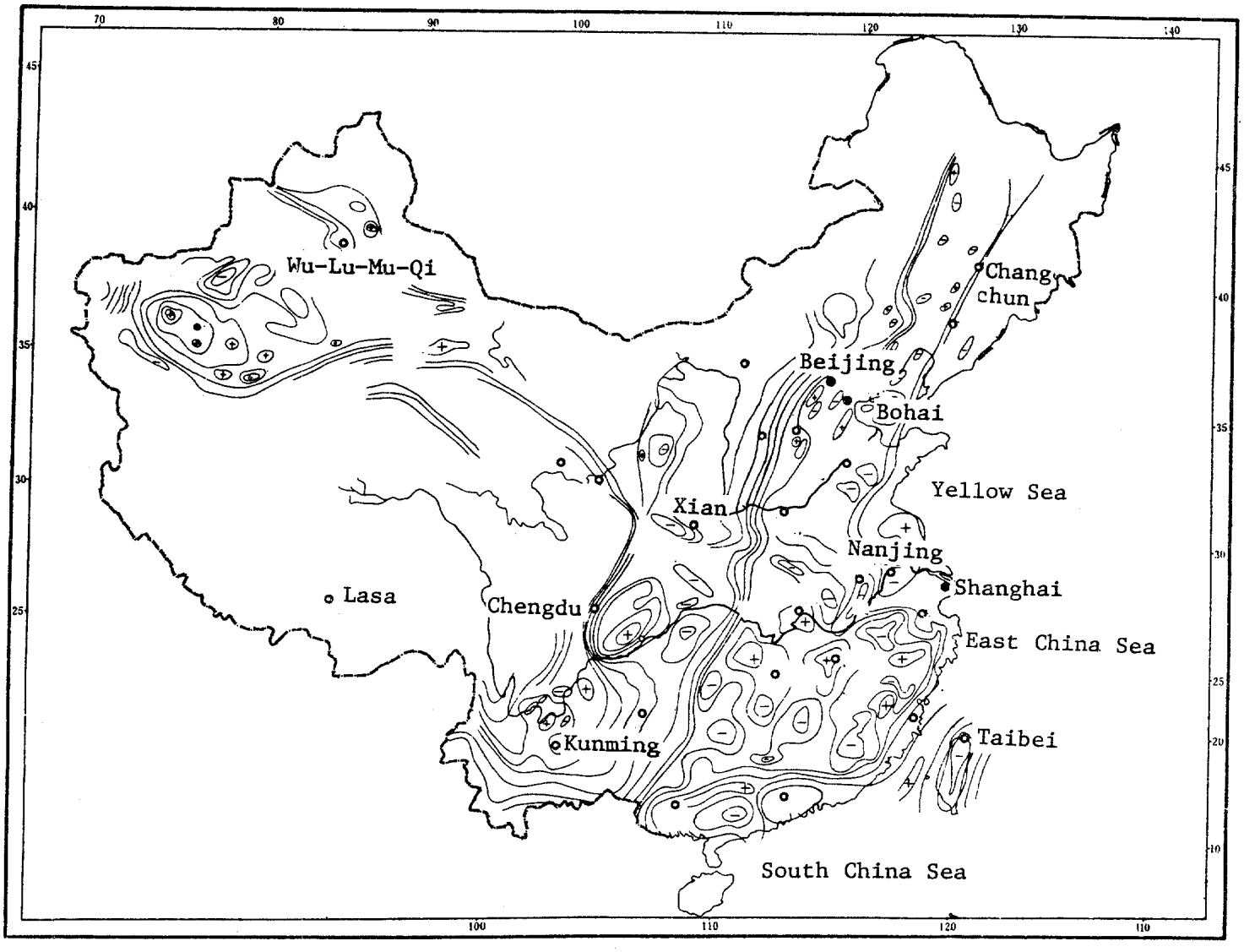

Figure 4: Map of Bouguer Gravity for portions of China.

From 1831 B.C. to A.D. 1980, 4,117 earthquakes with magnitude greater than 4 3/4 have been documented reliably as occurring in China. Of these, only 15 events are certainly or probably tsunamigenic. These are listed in Table 1, together with earthquake epicenter location, date, magnitude, intensity, and other relevant information. Most of the listed events occurred in ancient times when only the phenomena of sea-water motions caused by the earthquakes were observed, without any documentation of important parameters such as tsunami generation, water height, or period of the tsunami waves. The earthquake information shown in Table 1 should be compared with other catalogs of tsunamis.

For the determination of earthquake epicenters prior to this century, for which no seismic recordings were available, the epicenter is presumed to be in the region of heaviest destruction. As the county was often used in the historical record as the reference location, we have assumed the seat of each county to be the location of the earthquake epicenter. When isoseismal lines could be drawn, we took the geometric center of the isoseisms as the reference location for the epicenter.

Values of seismic intensity were determined from evaluation of the Table of Simplified Historical Earthquake Intensity and Magnitude (Nat.

TABLE 1. TSUNAMIS IN CHINA,
47 B.C. to A.D. 1978

DATE	GENERATION AREA	EPICENTER	MAGNITUDE	INTENSITY
47 B.C Sept.	Laizhou Bay, Bohai Sea			
173 A.D. June 27 July 26	Offshore of Huang, county, Shandong Province			
1046 April 24	Penglai coast, Shandong Province	37.8°N 120.7°E	5	6
1324 Sept. 23 (?)	Wenzhou, Zhejiang Province			
1344 Aug. 17 (?)	Wenzhou coast, Zhejiang Province			
1604 Dec. 29	Offshore Quanzhou, Fujian Province	25.0°N 119.5°E	8	
1605 July 13	Qiongshan, Wenchang Guangdong Province	19.9°N 110.5°E	7.5	10
1641 Sept. 16 - Nov. 26	Chenghai, Chuoyang Guangdong Province	23.5°N 116.5°E	5.75	7
1661 Feb. 15	South of Taiwan	23.0°N 120.2°E	6.0	7.5
1668 July 25	Juxian, Dancheng Shandong Province	35.3°N 118.6°E	8.5	12
1721 Sept. (?)	Tainan			
1792 Aug. 9	Jiayi, Taiwan	23.6°N 120.5°E	6.75	9
1867 Dec. 18	Jilong, Taiwan	25.5°N 121.7°E	(6) (6)	
1918 Feb. 13	Shantou, Nano	24.0°N	7.3	10
14hr-07m-13sec	Guangdong Province	117.0°E		
1921 Aug. 4	Xiaosi, Dandong Liaoning Province			

NOTE: On the basis of additional descriptive texts, the three earthquakes denoted by question mark (?) in Table 1 seem to have occurred while a storm surge due to a hurricane was in progress.

Bur. Seismology, unknown) and the Table of New China Intensity (Xie Yushou 1957). These tables have been empirically developed within China as references for evaluation of earthquakes. For earthquakes prior to 1900 for which magnitudes cannot be determined from seismograms, the intensity of the epicenter was drawn according to the historical record and the Table of Simplified Historical Earthquake Intensity and Magnitude. At the same time, the approximate magnitude of the earthquake was determined from the correlative formula of intensity and magnitude, i.e., $M = 0.58 I_o + 1.5$. Then it was checked and evaluated again by the size of the affected earthquake area; the final value for the magnitude was derived by comparative checking and correcting.

A map of China showing nine of the locations of the epicenters of the 15 tsunami-related events is given in Figure 5 (base map taken from the frontispiece of National Bureau of Seismology, 1983); the other six epicenters are unknown. Note that some of the epicenters are inland. It can be seen that tsunamigenic earthquakes occur most frequently along the southeastern coast of China and Taiwan. These earthquakes are of high intensity and shallow depth as proven by the historical record, and they are associated with faults having vertical crustal displacements.

In the lower part of Figure 6 (after Figure IX-3 of China Seismic Intensity Report, Nat. Bur. Seismology, 1981) is shown the magnitude-versus-time distribution for all earthquakes along the southeast coastal area of China. Note the extreme irregularity over time of these earthquakes. In the upper part of Figure 6 is given the magnitude-versus-time distribution for those tsunamigenic earthquakes listed in Table 1. There appears to be nothing unique about this distribution, perhaps simply for lack of dense data, although a few events are concentrated in the seventeenth century.

A few tsunamigenic earthquake events will be summarized as follows:

1. The earthquake of December 29, 1604. This earthquake occurred offshore of Quanzhou, Fujian province, (see Figure 1), as shown in Figure 7; its magnitude was large and its effects were widespread. The historical record reports (base map taken from Gu Gongxu et al., page 65, 1983) that "mountain, stone, and sea water were totally moving; many boats sank down; the ground was cracked apart."

This earthquake was generated along the seismic belt of the Fujian Guangdong coast. The west side of the seismic belt runs from Zhejiang province to Guangdong province. The geological cross-section of Changshan-Qinyingshan in Fujian province, as shown in Figure 8 (base map taken from China Seismic Intensity Report, Nat. Bur. Seismology, Figure IX-6, 1981) shows this belt to have transcurrent faults.

2. The earthquake of July 25, 1668. This earthquake was generated in the middle area between Juxian and Dancheng of Shandong province (see Figure 1) (Figure 9) (base map taken from Gu Gongxu et al., page 102, 1983) on a fault zone in the dominant uplift belt. The present characteristics of the faulting appear to be compressive thrusts, as shown in Figure 10 (adapted from a Figure of the China Seismic Intensity Report, Nat. Bur. Seismology, Figure V-7, 1981).

3. The earthquake of August 9, 1792 was generated in Jiayi, Taiwan (see Figure 1). Although not strong, it caused serious damage; the historical record states that "water was uplifted several meters without wind, the field slumped down and water flooded in lower" (Gu et al., 1983,

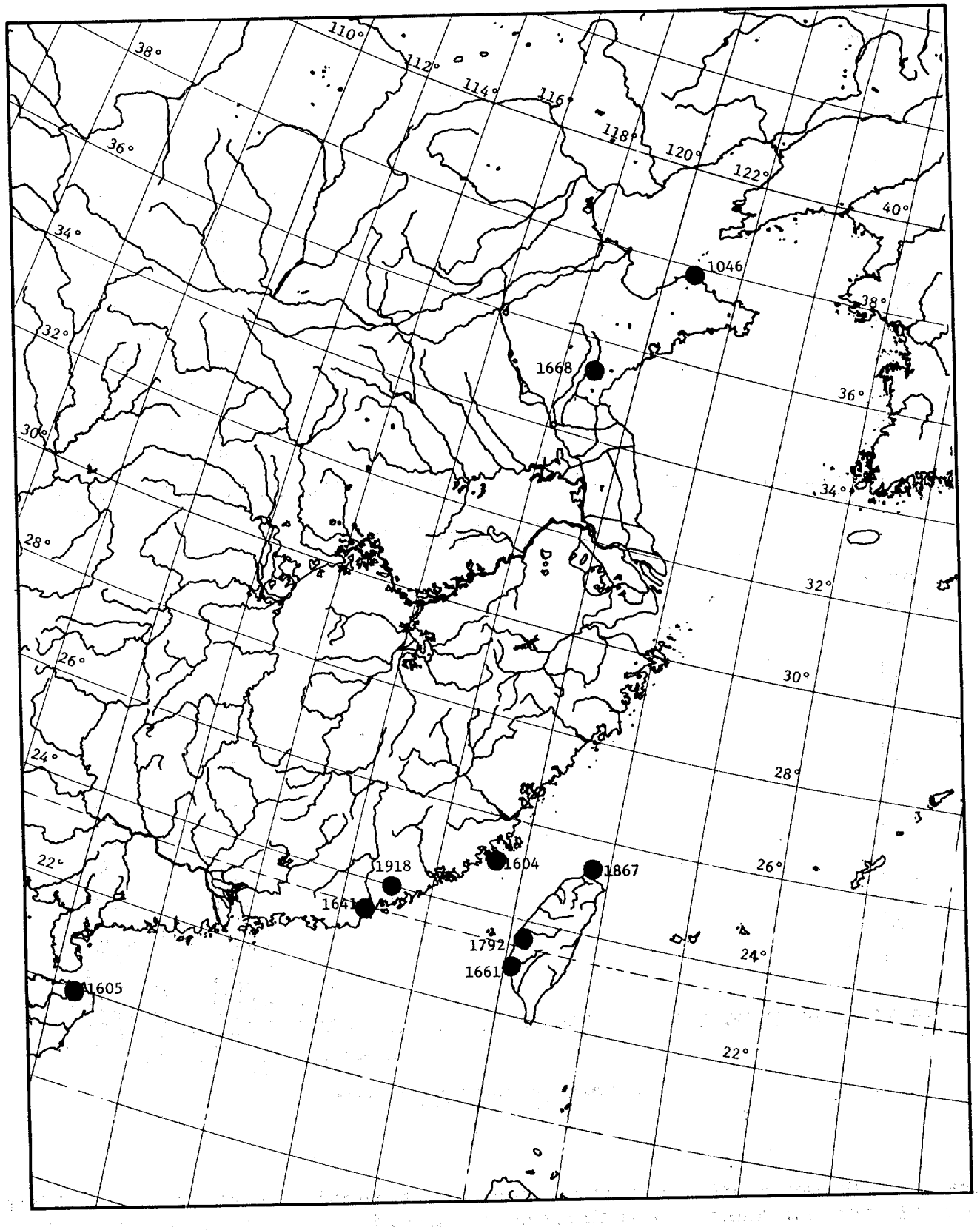

Figure 5: Map showing location of estimated epicenters for the known tsunamigenic earthquakes in China.

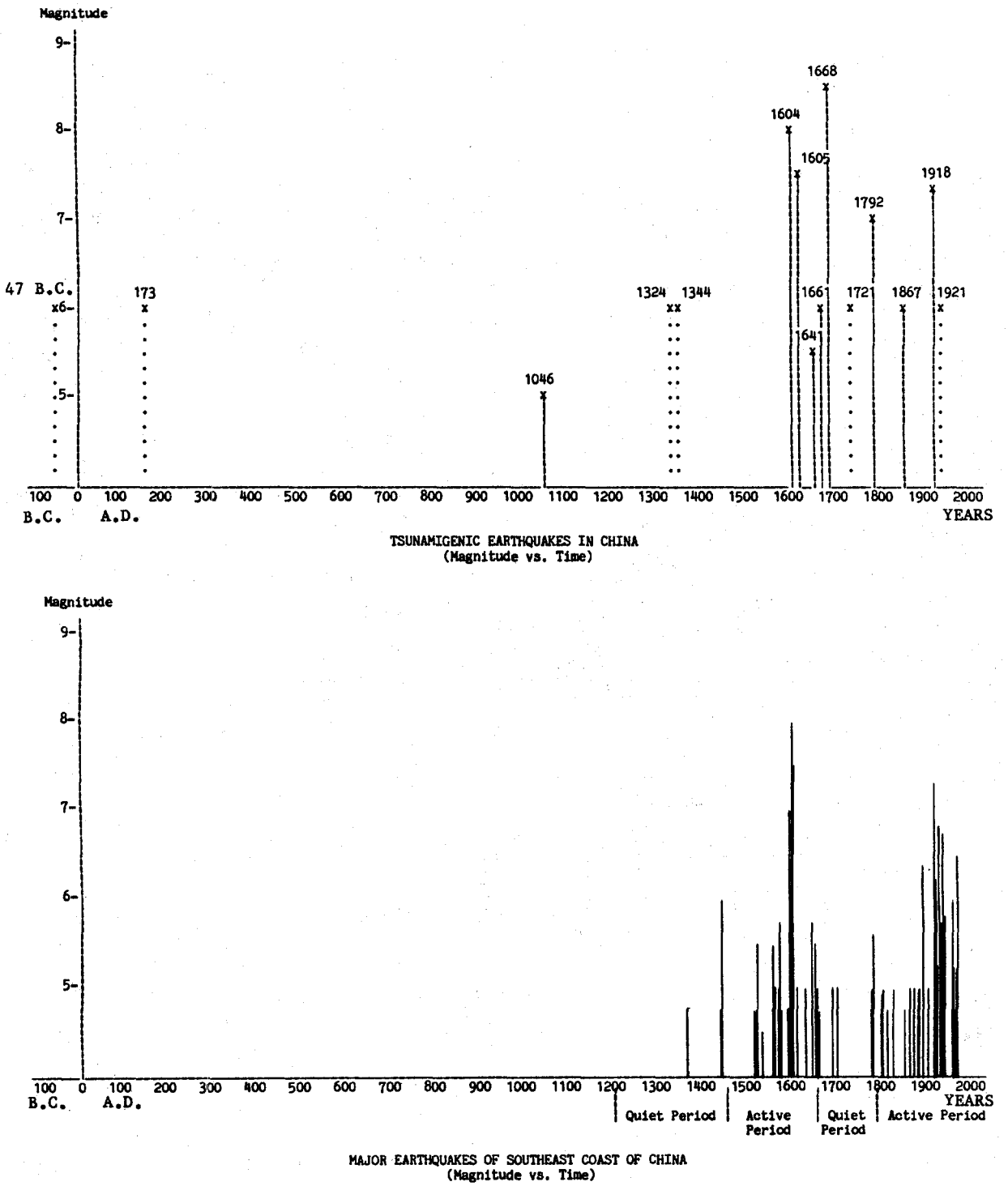

Figure 6: (Upper graph) For the known tsunamigenic earthquakes of China, a plot of the estimated earthquake magnitude as a function of time. No cyclical pattern is apparent.

(Lower graph) For the known major earthquakes having epicenters off or on the Southeast Coast of China, a plot of the estimated earthquake magnitude as a function of time. The alternation of quiet and active periods is indicated.

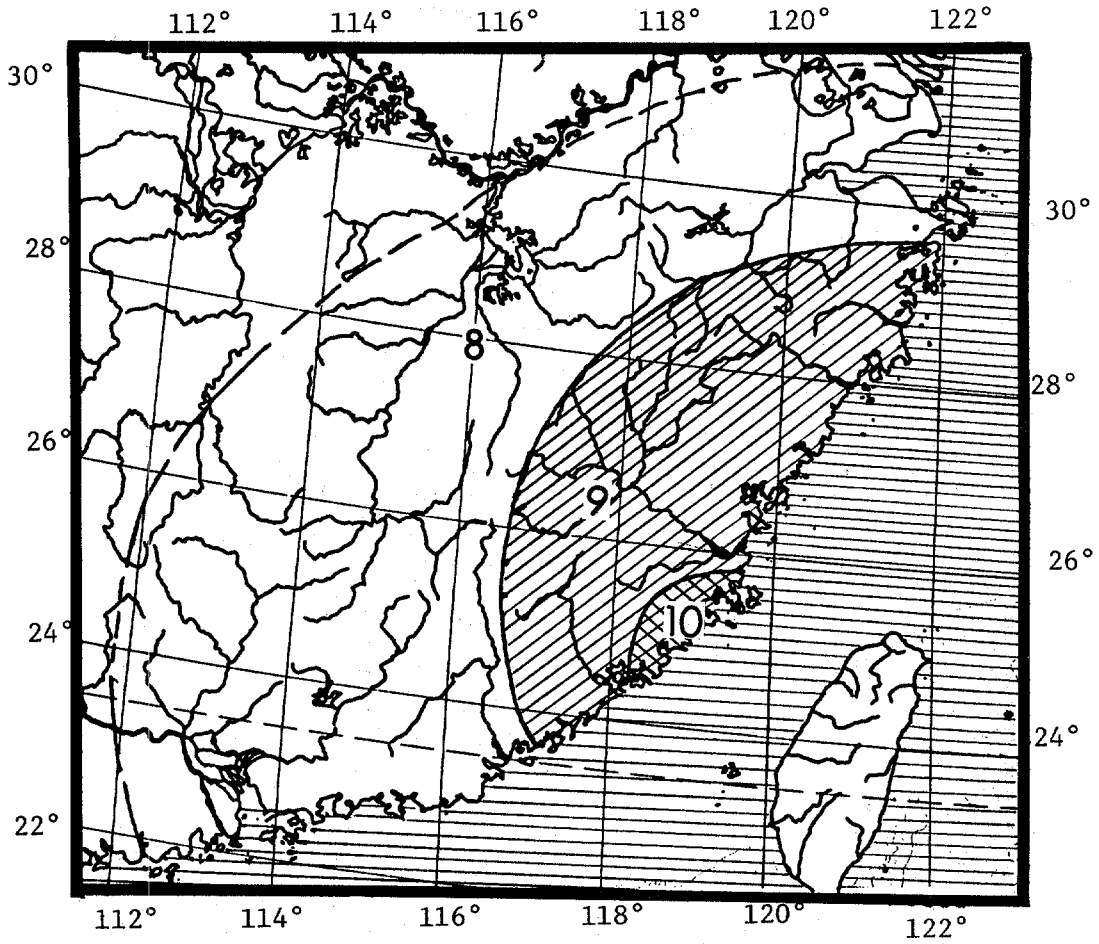

Figure 7: Map showing the isoseismal areas for the earthquake of December 29, 1604. The Chinese scale of intensity is used. (see Appendix)

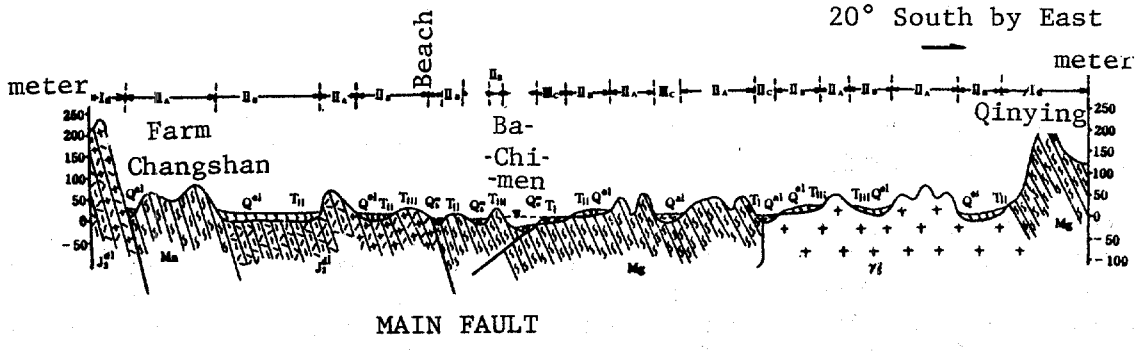

Figure 8: Geological cross-section of Changshan-Qinyingshan in Fujian, showing the setting of the main fault.

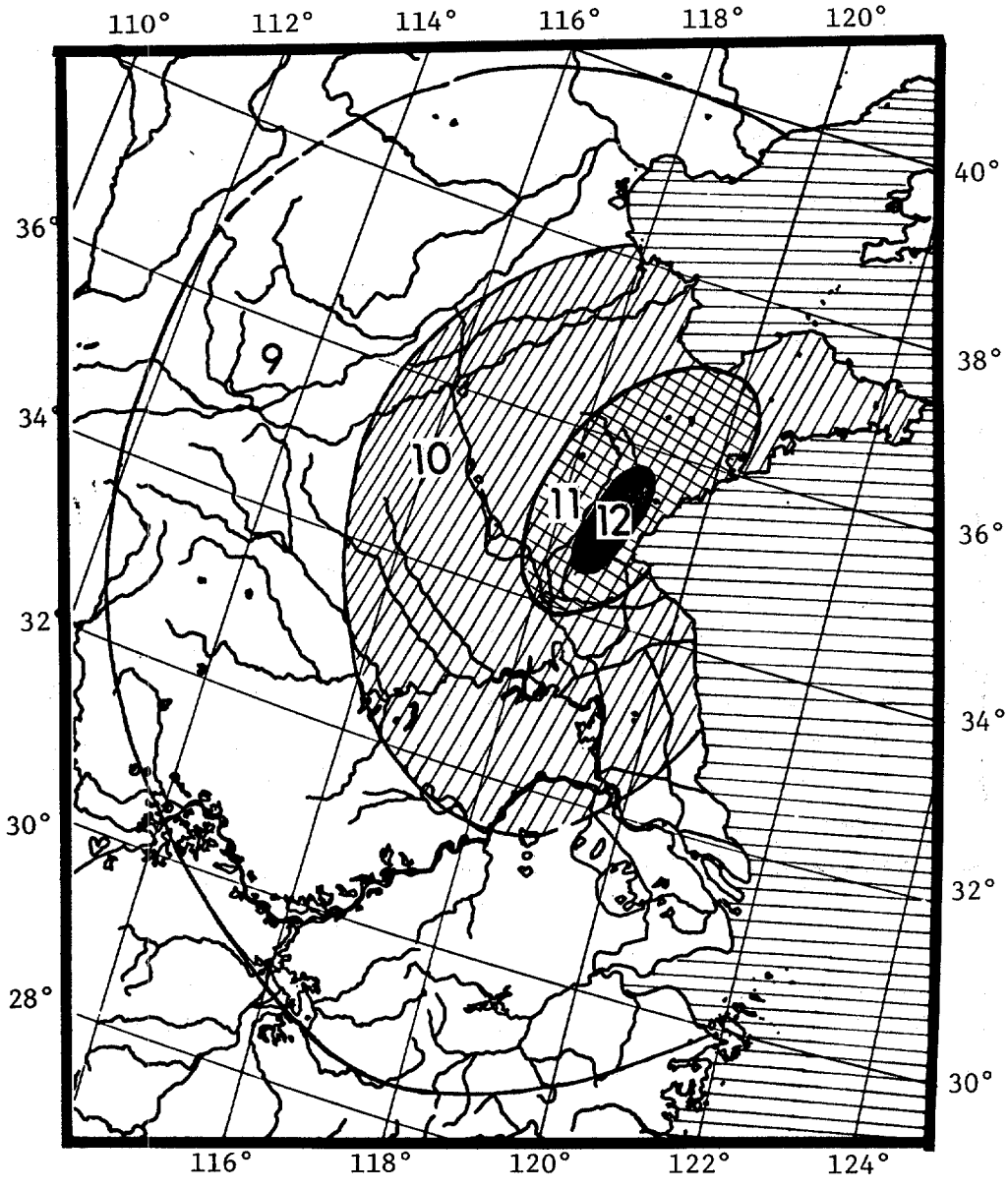

Figure 9: Map showing the isoseismal areas for the earthquake of July 25, 1668. The Chinese scale of intensity is used. (see Appendix)

pg. 144). Perhaps the shallow depth of the earthquake was a large factor in the damage it caused.

A cross section near the epicenter is given in Figure 11 (adapted from Figure VII-3 of the China Seismic Intensity Report, Nat. Bur. Seismology, 1981), showing that this earthquake was generated on a transcurrent fault. The structural geology and sedimentary thickness is shown in Figure 12 (adapted from figure V-3 of the National Bureau of Seismology, 1981a) for the area of Jaiyi, Taiwan, where four additional historical earthquakes (M > 6) have been centered along this transcurrent fault. These observations indicate the repetitiveness of the epicenters. The location of a tsunamigenic earthquake on a fault that evidences dominantly transcurrent faulting is surprising and should be further investigated.

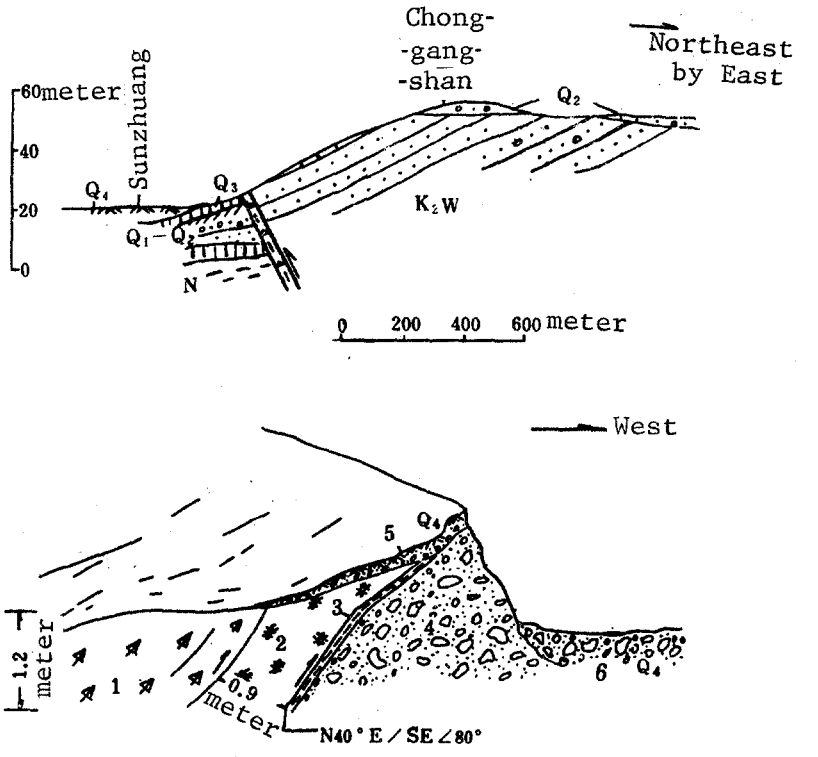

Figure 10: (Upper) Gross cross-section and (Lower) detail cross-section of the Dancheng-Lujiang Fault. (Note the reversal in orientation between the top and lower sections.)

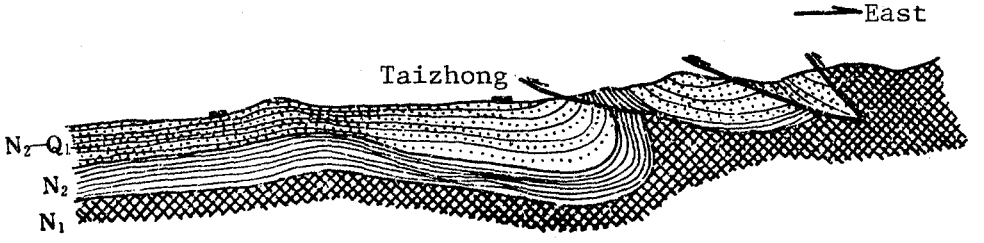

Figure 11: Geological Cross-Section of the Taizhong Basin

4. The earthquake of February 13, 1918. As shown in Figure 13 (adapted from the Figure 122 of Gu Gongxu et al., 1983), this high-intensity earthquake was generated in Nano, Guangdong province (see Figure 1) and caused extensive damage. The earthquake was generated on the seismic belt of the Fujian-Guangdong coast, similar to the geological setting of the event of December 29, 1604. The geological cross section of the Changshan-Qinyingshan of Fujian (Figure 8) described a transcurrent direction for this belt. Further, this earthquake was also located at the area near the Zhenghe-Haifeng (see Figure 1) fault zone, as shown in Figure 14 (Nat. Bur. Seismology, Figure V-8-a, 1981a). Here the fault zone appears to be compressive and to have rotated counter-clockwise.

In addition the effects of an earthquake on May 26, 1983, in the Sea of Japan were observed in areas of the North and East China Sea. For instance, a tide station near Shanghai recorded a water surge of 42 cm at 8:00 to 9:00 p.m. that night. Although it cannot be absolutely

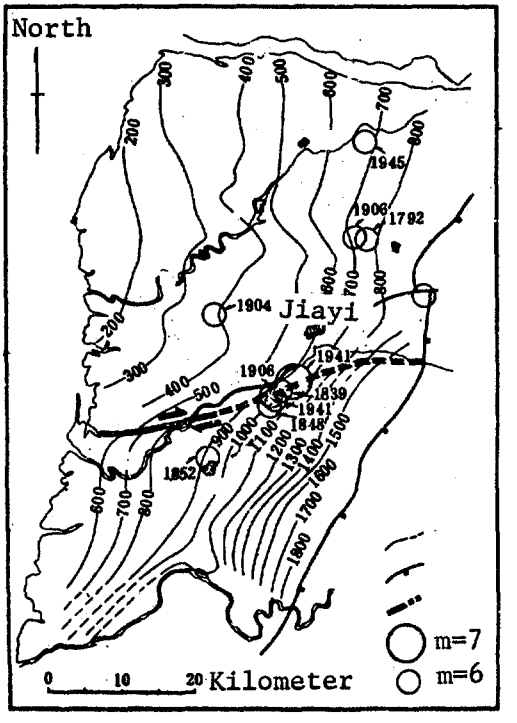

Figure 12: Map of the Geological Structure and Sedimentary Isopach for Jaiyi, Taiwan. The contours of the isopach are in meters of thickness.

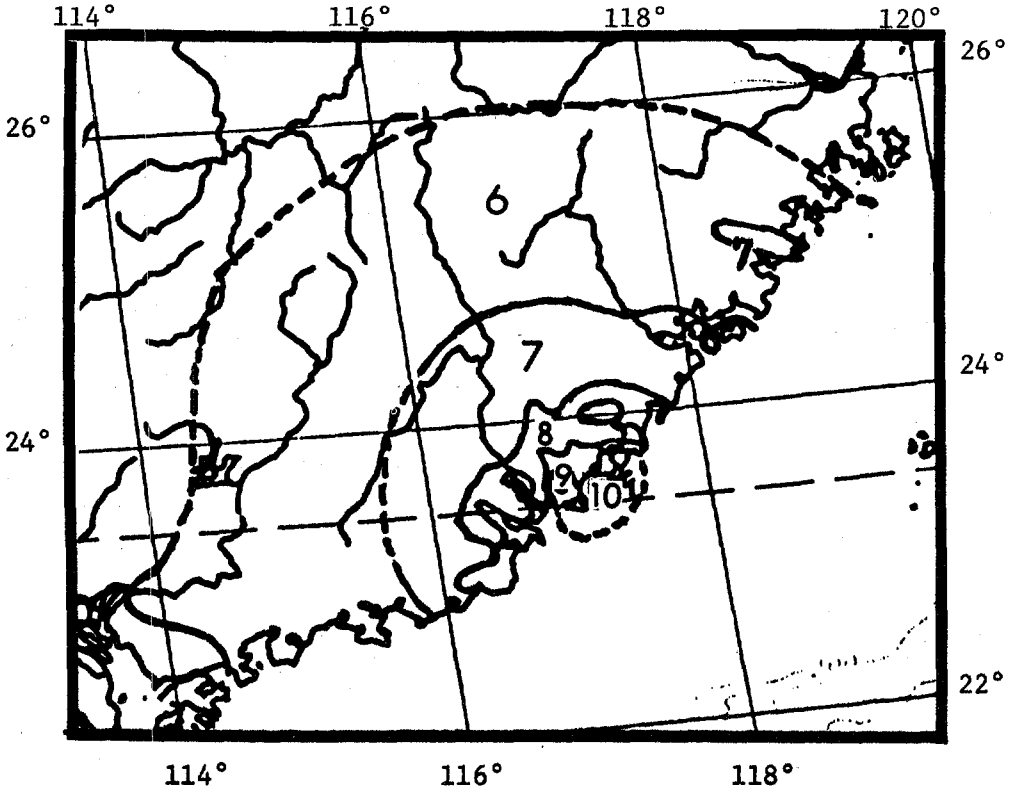

Figure 13: Map of the isoseimals for the Earthquake of February 13, 1918. The Chinese scale of intensity is used. (see Appendix)

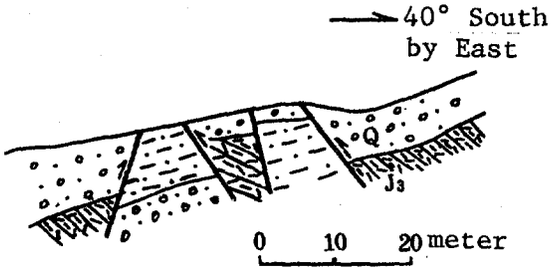

Figure 14: Geological cross-section of the Zhenghe-Haifeng Fault.

demonstrated that the surge was associated with that earthquake, it can be shown that the tsunami waves generated by that earthquake reached the coastal area of China near Shanghai.

III. DATA BASE

"Perfect Filer", a database system from the Perfect Software System (Perfect Software Inc., 1983), is being used at Hawaii Institute of Geophysics for formatting input on tsunamigenic earthquakes in China and control events. Control events are earthquakes that have many similar parameters, such as source location and magnitude, similar to those of tsunamigenic earthquakes but that are not tsunamigenic.

The format being used in this simple database is fixed field lengths, as given Table 2. The data in each field are specified, together with the number of alphanumeric or numeric characters. As "Filer" also has automatic range-checking for numeric fields of fewer than five characters, the range being used for each field parameter is given for the appropriate fields.

The purpose of this study and the preparation of this database (which is presently being run on a Pied Piper computer) is to form a basis from which to develop zonation maps of tsunami hazard for the coastal areas of China (Zhou and Adams, 1986a, 1986b).

IV. CONCLUSION

From historical information concerning tsunamigenic earthquakes in China we can see that the generation of tsunamis in China is infrequent, but possible. Analysis of this possibility will be given in this series of papers.

ACKNOWLEDGMENTS

This work has been aided by materials on some geological features of China provided by Pow-foong Fan. Funding for presentation in Vancouver, B.C., was arranged by the China - U.S.A. Bilateral Scientific Interchange Agreement. Discussions with George Pararas-Carayannis, Gordon Burton, and others concerning the validity and quality of the data have been most helpful. Evelyn Norris and Bethanee Austin provided word processing; both Gordon Burton and Rita Pujalet provided expert and conscientious editing. Hawaii Institute of Geophysics Contribution no. 1661.

TABLE 2. DATA BASE FORMAT

FIELD	LENGTH	TAGS	RANGE
First	5	Year	-2000 to 1990
Second	2	Month	1 - 12
Third	2	Day Zone time	1 - 30
Fourth	2	Hour (local time)	0 - 23
Fifth	2	Minute	0 - 59
Sixth	2	Second	0 - 59
Seventh	7	Era	
Eighth	2	Year Japanese Time	0 - 50
Ninth	2	Month	1 - 12
Tenth	2	Day	1 - 12
Eleventh	5	Year	-2000 to 1990
Twelfth	2	Month Chinese Time	1 - 12
Thirteenth	2	Day	1 - 31
Fourteenth	10		
Fifteen	10	Latitude	
Sixteenth	1	+ (north) or - (south)	
Seventeenth	10	Longitude	
Eighteenth	1	+ (east) or - (west)	
Nineteenth	3	Standard deviation of space	0 - 999
Twentieth	3	Standard deviation of time	0 - 999
Twenty-first	4	Magnitude	0 - 6
Twenty-second	3	Standard deviation of magnitude	0 - 999
Twenty-third	3	Depth	0 - 700
Twenty-fourth	4	Standard deviation of depth	0 - 999
Twenty-fifth	2	Peak intensity (Modified Mercalli)	0 - 12
Twenty-sixth	1	Region	
Twenty-seventh	15	Origin Area	
Twenty-eighth	4	Tsunami magnitude ($m = \log_2 H$)	0 - 7
Twenty-ninth	10	Terminal area	
Thirtieth	4	Maximum runup (For H location)	0 - 40
Thirty-first	5	Travel time	
Thirty-second	2	Period of maximum energy (minutes)	0 - 60
Thirty-third	10	Additional data (observed)	
Thirty-fourth	20	Reference (For H location)	
Thirty-fifth	10	Additional reference	
Thirty-sixth	5	Peak acceleration	

REFERENCES

Fan, Pow-foong, 1986a, "Geology of China," Encyclopedia of World Regional Geology. Part 2: Eastern Hemisphere (Vol. VIII). Edited by Rhodes W. Fairbridge, to be published by Dowden, Hutchinson Ross Inc.

Fan, Pow-foong, 1986b, "Geomorphology of China," Encyclopedia of World Regional Geology. Part 2: Eastern Hemisphere (Vol. VIII). Edited by Rhodes W. Fairbridge, to be published by Dowden, Hutchinson Ross Inc.

REFERENCES

Gu Gongxu, G., Lin Tinghuang, Si ZhenLiang, Li Qun, Wu Huanying, Lu Shoude, Yang YuLin, Chen HaiTong, Wang Suyun, 1983, Catalog of Earthquakes in China, National Bureau of Seismology, 894 pp. (in Chinese).

Li, Tingdon, 1980, The Development of Geological Structures in China, GeoJournal, vol. 1, no. 6, pp. 487-497.

National Bureau of Seismology, 1981a, China Seismic Intensity Report, Published by National Bureau of Seismology (in Chinese).

National Bureau of Seismology, 1981b, Table of Simplified Historical Earthquake Intensity and Magnitude, and Table of New China Intensity (in Chinese).

Perfect Software, 1983, "Perfect Filer" by Perfect Software, Inc., 1983. 1400 Shattuck Avenue, Berkeley, CA 94709.

Xie Yushou, 1957, Table of New China Intensity, National Bureau of Seismology.

Xie Yushou and Cai Meipiao, 1983, Historical Earthquake Information Compilation in China, 277 p. (in Chinese).

Zhang, Zh. M, J. G. Liou, and R. G. Coleman, 1984, An outline of the plate tectonics of China, Bulletin of the Geological Society of America, v. 95, pp. 295-312.

Zhou, Qinghai, and W. M. Adams, 1986a, Database of Tsunamigenic Earthquakes in China, presented at Pacific Congress on Marine Technology, 24-28 March, Honolulu, Hawaii; extended abstract in the Program.

Zhou, Qinghai, and W. M. Adams, 1986b, Preliminary Zonation of Some Populated Coastal Sections of China for Tsunami Hazard, to be presented at the International Symposium on Natural and Man-Made Hazards, August 1986, Rimouski and Quebec City, Canada.

APPENDIX

Some portions of three intensity scales are compared. This covers the acceleration range from 1 to 1000 gals. The upper scale is the Japanese scale of intensity; the middle scale is the common Modified Mercalli; and the lower scale is the Chinese scale of intensity. Note that the Chinese scale is not partioned below 10 gals as the authors do not have information for that range. Arabic numerals are used for the Chinese scale of intensity and have been used in the figures in this article; however, perhaps the standard use of Roman numerals should be followed.

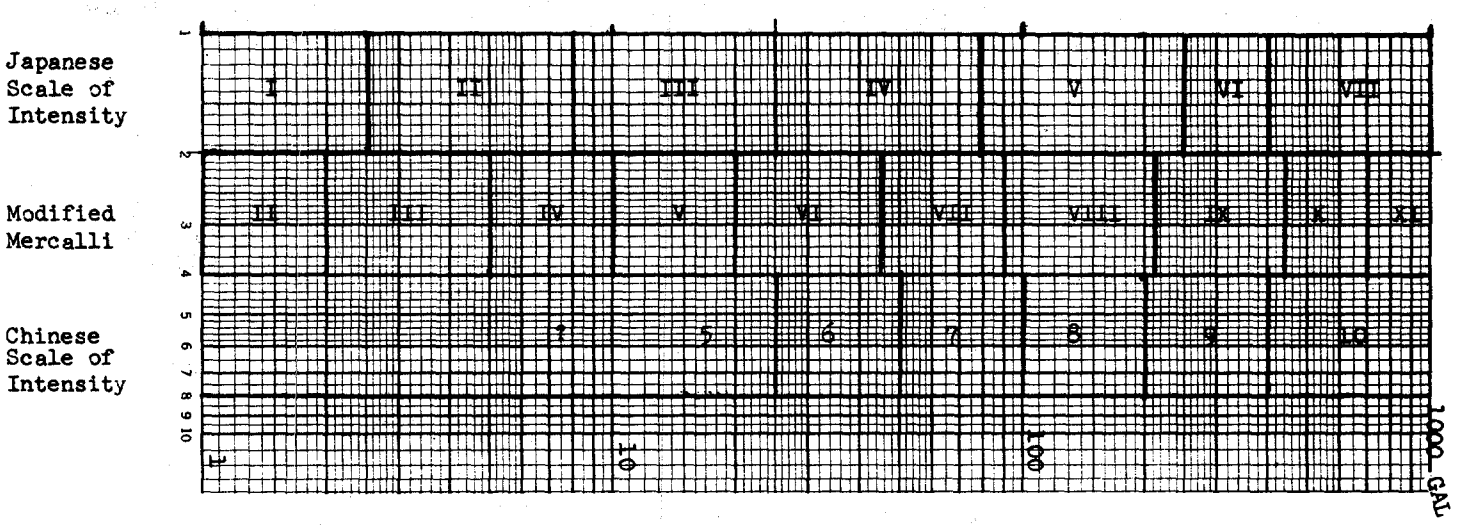

PROPAGATION OF TSUNAMI WAVES GENERATED BY ELLIPTICAL SOURCES

V.M.Galkin, V.I.Golin'ko, V.I.Malizhenkova, N.R.Mirchina, E.N.Pelinovsky

Institute of Applied Physics USSR Academy of Science, Gorky, USSR

Tsunami sources are known to be elongated along the continental slope and they are approximated by ellipses. Meanwhile the theoretical calculations of tsunami waves are usually made for idealized sources in the form of strips or circles. Since the tsunami sources in the Kuril-Kamchatka zone are at the long axis distance from the shoreline the one-dimensional calculations for a striped source or the asymptotic formulae of the cylindrical wave theory for a circular source have to be validated. The available numerical calculations for tsunami waves generated by elliptic sources in basins of variable depth relating to real tsunamis are too different to follow the formation of tsunami waves by elliptic sources as an independent process. The purpose of this paper is to investigate in model conditions (ocean of constant depth, homogeneous displacement in the source) the dependence of the tsunami wave characteristics on distance from the origin, source orientation, its eccentricity, nonlinearity and dispersion parameters. These results are used to estimate the applicability of known theoretical models.

The formation of tsunami waves by elliptic sources may be devided into two stages (such an approach is well known for nonlinear waves): in the first stage (near the source), the nonlinear and dispersion effects are neglible and, therefore, the process can be described in terms of the shallow-water linear theory; in the second stage, these effects accumulate in the course of the wave propagation and the process is described by the nonlinear ray methods. Consider the first stage of the tsunami formation.

As is well known, the general solution of the Cauchy-Poisson problem in the shallow-water linear theory approximation is of the form :

$$\zeta(x,y,t)=\frac{1}{2\pi}\frac{\partial}{\partial t}\iint_{\sigma_t}\frac{\zeta_0(\xi,\eta)\,d\xi\,d\eta}{\sqrt{c^2t^2-(\xi-x)^2-(\eta-y)^2}} \qquad (1)$$

where $\zeta(x,y)$ is the level disturbance at the initial moment, $c=\sqrt{gh}$ h=const is the ocean depth, g is the gravitational acceleration. Integration in (I) is made over the circle σ_t :

$$(\xi-x)^2+(\eta-y)^2 \le c^2t^2 \qquad (2)$$

For simplicity's sake we consider a homogeneous disturbance:

$$\zeta_0(x,y)=\begin{cases}\zeta_0 & \frac{x^2}{a^2}+\frac{y^2}{b^2}\le 1\\ 0 & \frac{x^2}{a^2}+\frac{y^2}{b^2}>1\end{cases} \qquad (3)$$

First we list the results for striped and circular sources. As is known, in the case of a striped source ($a = \infty$) the wave retains its initial form of a rectangle of length 2b and height $\zeta_0/2$. The numerical calculations according to (1) indicate that the wave produced by a circular source ($a=b=R_0$) has an universal form independent of r. Moreover, the positive phase is always replaced by the negative phase, in contrast to the one-dimensional case of a striped source. Thus, for the wave amplitude (field jump on the wave front) we have found the formula:

$$\zeta_m = 0{,}5\,\zeta_0\sqrt{R_0/r} \qquad r \gg R_0 \tag{4}$$

The positive phase wavelength λ_p is equal to 1.6 Ro. Strictly speaking, the wave negative phase has an infinite duration. At $t \gg (r+R_0)/c$ the well-known formula is valid :

$$\zeta = -\zeta_0 R_0^2 / 2c^2t^2 \tag{5}$$

At last we note that for $t = (R_0+r)/c$ the marigram has an unlimited negative pulse caused exclusively by the chosen form of initial disturbance (by $\zeta_0(r)$ rupture at r=Ro). The field is restricted everywhere for smooth initial disturbances.

Some of the results mentioned here (negative phase existence, the dependence $\xi \sim r^{-1/2}$ for large r) have already been cited in literature.

The analytical results obtained from (1) for an elliptic source are not so numerous. The most important of them is the formula for wave front amplitude :

$$\zeta_m = 0{,}5\,\zeta_0\sqrt{R/d} \tag{6}$$

where R is the curvature radius of the ellipsis at the point nearest to the point of observation; d is the distance from the observational point to the center of the circle of curvature R^{-1}. Formula (6) is valid at any distance r from the observational point to the center of the source ($r > r_3$). For $r \gg a$, a formula analogous to (6) was first obtained by Kajiura, which can be put into a convenient form :

$$\zeta_\infty(r,\alpha) = 0{,}5\,\zeta_0\sqrt{R(\alpha)/r} \tag{7}$$

where α is the angle reckoned from the long axis direction. As follows from (7) the amplitude again decays as $r^{-1/2}$ but depends on the source orientation α relative to the observational point and on the source configuration. The negative wave phase has an infinite duration as in the case of a circular source, and at $t \gg (r+a)/c$

$$\zeta \simeq -\zeta_0\, ab/2c^2t^2 \tag{8}$$

It can be shown that the negative phase contains an infinite-amplitude pulse (sometimes two pulses may occur), where the field has a logarithmic divergence, arising from the specific initial conditions.

To investigate the formation of tsunami waves by elliptical sources, numerical calculations have been carried out for a number of ellipsis axis ratios b/a, distances from the ellipse r/a and angles α reckoned from the long axis direction. Thus, the marigrams obtained numerically permit one to conclude:

1. The form of the main energy-containing wave train depends on the distance only for $r \lesssim (5 \div 10)a$. At larger distances the wave takes an asymtotic form (which does not change with distance), and the wave amplitude is given by (7).

2. At large distances (in the asymptotic regime) the wave has a universal form for appropriate variation of the horizontal and vertical scales, in accord with Kajiura's results.

3. At small distances for strongly elongated sources, the positive wave phase has a form similar to that of the initial disturbance, and the wave amplitude almost does not change in a direction close to the small axis (as in the one-dimensional case). Meanwhile the negative phase is again present.

The existence of the negative phase is very important to make a proper choice of the form of the initial disturbance when dealing with the tsunami zonation. Since the shelf zone has resonance properties, tsunami run-up depends on the form of the initial disturbance. In the preliminary schemes of tsunami zonation of the Kuril-Kamchatka region one-dimensional calculations for the source motion of constant sign were used. Since the tsunami sources are located near the shoreline, the one-dimensional approximation should be valid, but the form of the source disturbance has, in view of our model calculations, to be replaced by an alternating one. The same suggestion follows from the seismic Alekseev-Gus'akov's model.

Further, the investigation of the second stage of tsunami propagation (when nonlinearity and dispersion have to be taken into account) has been carried out in the framework of Korteweg-de Vries equations. It has been shown that the characteristics of the wave propagation (Ursell number U, the lengths of nonlinearity L_N and dispersion L_Φ) significantly depend on the source orientation. Estimates of U, L_Φ, L_N in the directions of the main axes for a number of past tsunamis have been tabulated to make definite conclusions using natural data. As is evident from the Table, the nonlinear dispersion theory is significant for the description of many tsunami events.

Date	Location	U_a/U_s	L_{Da}/L_{Ds} ts.km	L_{Na}/L_{Ns} ts.km
15.06.1896	Sanriku	0.7/0.77	3.3/5.7	-/-
27.05.1928	Iwate	0.1/0.11	0.24/0.48	-/-
09.03.1931	E.Aomori	0.7/1.4	0.06/4.3	-/13
02.03.1933	Sanriku	0.1/0.2	0.3/12.5	-/-
19.06.1933	Miyagi	0.1/0.1	0.5/0.5	-/-
13.10.1935	Iwate	0.1/0.1	0.9/0.9	-/-
02.11.1936	Sanriku	5.0/6.7	0.5/3.2	0.4/1.9
23.05.1938	Ibaraki	1.3/1.5	0.6/2.2	3/5,6
05.11.1938	Fukushima	2.7/3.1	2.6/5.7	3.9/7.4
13.11.1938	Fukushima	2.4/2.9	0.6/1.1	1.1/1.5
01.05.1939	Oga	4.2/4.5	1.4/2.1	1.3/1.8
01.08.1940	W.Hokkaido	0.07/0.08	0.8/2.4	-/-
07.12.1944	Tonankai	2.4/3.1	0.96/5.6	1.6/7.4
20.12.1946	Nankaido	0.06/0.2	0.01/21.3	-/-
04.03.1952	Tokachi-Oki	34.6/45.0	-/-	0.2/0.8
04.11.1952	Kamchatka	0.5/1.1	0.5/56	-/206
25.11.1953	Boso-Oki	0.01/0.01	0.04/0.04	-/-
22.05.1960	Chili	0.7/1.3	2/102	-/51
27.03.1964	Alaska	11.3/21.5	-/-	0.2/5.1
16.06.1964	Niigata	26/39	-/-	0.3/1.7
16.05.1968	Tokachi-Oki	0.7/0.9	0.5/2.1	-/-

AN EXPLANATION OF CHARACTERISTIC DISTRIBUTION OF THE TSUNAMI MAXIMUM INUNDATION HEIGHTS OBSERVED AT THE SMALL ISLANDS

Kuniaki Abe
General Education, Nippon Dental University, Niigata
Hamaura-cho 1-8, Niigata, 951, JAPAN

ABSTRACT

The harmonic responses of plane wave to the Okushiri and Awashima Islands in the Japan Sea were obtained by the use of finite element method and the amplitude distributions obtained for various frequencies were compared with those of the maximum inundation heights observed at the coasts of these islands in the 1983 Japan Sea Tsunami. The comparison suggested the incidence of wave having the frequency component of 1.4-1.5 $x10^{-3}$ Hz. The result is supported by the fact that the component wave was detected in the initial stages observed by many tide gages installed at the coasts of the Honshu Island. The component wave is attributed to the source condition and the role of the intermediate sea depth is pointed out.

The spectral peak observed by the tide gage at the Awashima Island is explained by the amplitude distribution calculated as an excitation of natural oscillation between the island and the Honshu Island.

Introduction

Recently some investigators applied a finite element method to the tsunami. Houston(1978) solved the extended Helmholtz equation of sinusoidal wave applying it to the Hawaiian Islands and compared the observed tsunami with the wave forms synthesized by the use of the obtained result. Kawahara(1978) developed the finite element method to deal with the time historical problem of the 1952 Tokachi-oki Tsunami.

Since the tsunami is a transient phenominon, it goes without saying that it is important to discuss the wave form. At the same time it is also important to study the interaction to the island from the view point of sinusoidal wave.

The 1983 Japan Sea Tsunami showed us many noticeable motions. One of them was higher elevations of the wave observed at the tips of the small islands. Sakai(1984) computed the time histories of the sinusoidal waves around the Oki Island to explain the topographic effect of the island to the 1983 Japan Sea Tsunami by the use of finite difference method. He dealt the periods ranging from 5 to 10 min and qualitatively showed a superiority of 7 min to simulate the distribution of the maximum inundation heights. In the small islands the tsunami attained to the level at the coast facing to the incident direction higher than that at the coast of Honshu having the same epicentral distance(Abe and Ishii, 1983). This fact suggests that the frequency of the tsunami was high enough to respond to the topographic change of the small island. To explain this characteristic distribution it is significant to investigate the harmonic response of the small islands by the use of the finite element method. In the harmonic analysis it is assumed that the time dependence is periodic.

We will deal with two cases of the small islands in Japan because of much data available. One is for the Okushiri Island located at the south west Hokkaido and another is for the Awashima Island located at the west part of the north east Honshu. The location map is shown in Fig.1. Particularly the former suffered from a great damage due to the invasion of the tsunami. The observation data are quantitatively compared with the computed result by the use of the correlation coefficients.

Basic equation

In a linear framework an extended Helmholtz equation for the sea surface $\eta(x,y)$ in the sea depth $h(x,y)$ is obtained assuming time dependence of $\exp(i\omega t)$ as follows:

$$\frac{\partial}{\partial x}\left(h\frac{\partial \eta}{\partial x}\right) + \frac{\partial}{\partial y}\left(h\frac{\partial \eta}{\partial y}\right) + \frac{\omega^2}{g}\eta = 0 \quad (1)$$

in which ω is angular frequency, g is gravity constant. The angular frequency is expressed by the use of frequency f. That is $\omega = 2\pi f$. Two kinds of boundary conditions are assumed. One is a unit amplitude condition in all the grid points on y axis representing the amplitude of incident plane wave. Another is a condition of no amplitude derivative normal to the boundary, which is expressed as follows;

$$u = \frac{\partial \eta}{\partial x}\cos\theta_x + \frac{\partial \eta}{\partial y}\cos\theta_y = 0 \quad (2)$$

in which θ_x and θ_y are the angles of a line normal to the boundary one for x and

y axes, respectively. This means no flow normal to the boundary, that is a total reflection. In this case the total reflection is not only applied to the coast but also applied to the calculation boundaries extending toward the direction of wave normal from the two side points on the y axis.

The sea areas including the objective islands are taken in the first quadrants and covered by the elements. For these wave fields the equation (1) is numerically solved under the boundary conditions for an assumed frequency and the harmonic solution $\eta(x,y)$ is obtained.

Results

(1) The Okushiri Island

The grid scheme for the Okushiri Island is shown in Fig.2. The model is consisted of 371 elements and 216 nodal points. The smallest one in all the intervals between the nearest neighbors is 2500 m. The azimuth angle of the incident direction was assumed to be N163°W from the application of the symmetrical distribution of amplitude for the cylindrical island obtained by Honma(1952) to the azimuthal distribution of the maximum inundation heights around the island observed in the Japan Sea Tsunami by Abe and Ishii(1983). The direction of x axis was selected to coincide this azimuth in the grid scheme. Accordingly the y axis corresponds to the wave front of the initial wave.

The unit amplitude is loaded to all the nodal points on the y axis. The calculation boundaries are set on both the sides along the wave normal of the initial wave predicted from the sea bottom topography to be kept far away from the island. For this grid scheme the amplitude fields are computed for the frequencies ranging from 1×10^{-4} Hz to 2.0×10^{-3} Hz at the interval of 1×10^{-4} Hz. One of the results computed for the frequency of 1.5×10^{-3} Hz is shown in Fig.3.

The result represents a concentration of wave energy to the south tip of the island, which was observed in the 1983 Japan Sea Tsunami as shown in Fig.4. The observation is due to Abe and Ishii(1983) and the values of the maximum inundation heights are expressed as the heights above the mean sea level. Their result is used as the base of comparison. In the comparison of amplitudes it is necessary to consider that the maximum inundation height above the mean sea level deviates from the maximum amplitude by the difference between the tidal level at the arrival time of the maximum inundation wave and the mean sea level. The difference cannot be reduced by reason of unknown arrival time of the maximum inundation wave. But the value is estimated to be in the range between high level and low one of the tide and is smaller than 0.3 m, which is predicted from the tide table. Accordingly the maximum error in the use of the height above the mean sea level is 0.3 m.

We pick up the amplitude values on the nodal points located at the coast of the island model from the amplitude field computed and make them correspond to the observed ones. If there is no corresponding point of observation, the computed one is abandoned. The inverse case is also possible. In the case of having dense observation points an average of the observed values is taken. Thus the pairs of amplitudes are listed up as many as the corresponding points. A correlation diagram is given for all the pairs of amplitudes. The result obtained for the frequency of 1.5×10^{-3} Hz is shown in Fig.5. The correlation coefficient is calculated to be 0.83 for the frequency.

The correlation coefficients between observation and computation are calculated for all the other frequencies and the frequency dependence of the correlation coefficients is obtained as shown in Fig.6. Since the space distribution of the maximum inundation heights depends on frequency, it is considered that the frequency dependence reflects the spectrum of the wave. It shows some peaks. Among them the most predominant frequency is 1.5×10^{-3} Hz and the maximum value is 0.84 as described above. The example, which was shown in Fig.5, is the case of the maximum correlation coefficient among all the cases.

(2) The Awashima Island

The same method as that was applied to the Okushiri Island was also applied to another small island, the Awashima Island. The island, being located on the shelf of the Honshu Island, has a linear dimension of 7 km. The model is constructed for the area including the island and the coast of the Honshu. The grid scheme, shown in Fig.7, consists of 399 elements and 231 nodal points. The shortest interval of the nearest neighbors is 625 m. The azimuth angle of incident direction is assumed to be N69°W. The x axis of the model is determined to coincide with the azimuth angle of the incident direction. The deviation of the incident direction from one of the source results from the refraction due to the the continental slope in front of the island. The calculation boundaries are taken to be parallel to the x axis. The amplitude distribution is computed for the incidence of unit amplitude at the grid points on the y axis.

One of the computed results is shown for the frequency of 1.4×10^{-3} Hz in Fig.8. The figure shows that the wave is moderately amplified at the coast facing to the outer sea and decreased in amplitude at the opposite side. The figure also shows that the waves are amplified at two corners surrounded by the calculation boundaries and the coast of the Honshu Island. It is considered that the latter amplification resulted from the superposition of waves at these corners because of the assumption of total reflection at the calculation boundary. The total reflection at the calculation boundary is an approximation neglecting the wave which propagates along the coastline of the Honshu Island. The increase of amplitude at the corners results from the approximation. Therefore it is necessary that the discussion of amplitude is restricted to the neighborhood of the island.

The maximum inundation heights observed by Abe and Ishii(1983) is shown in Fig.9. Their result is also used for the comparison. Since the values were measured on the basis of the mean sea level, the maximum error is 0.3 m, which is the difference between high tide and low one, on the same discussion as for the Okushiri model. The absolute values of amplitude computed at 15 nodal points on the coast of the island are picked out for each frequency and they are compared with the values observed. Thus the diagram of correlation relation between observation and computation is obtained for each frequency.

The comparisons are made for 20 cases of frequency. One example obtained for the frequency of 1.4×10^{-3} Hz is shown in Fig.10. The figure shows a good correlative relation. In fact the coefficient was obtained to be 0.90 and this value is the largest one among all the cases investigated. The correlation coefficients are shown as a function of frequency in Fig.11.

Significance of the correlative frequencies

The correlation coefficients of amplitude between observation and computation were obtained for both the models of Okushiri and Awashima as functions of frequency of sinusoidal waves. The maximum values were obtained for the frequencies of 1.5×10^{-3} Hz in the Okushiri model and 1.4×10^{-3} Hz in the Awashima model. It is shown that these two values almost coincide and the difference is 1×10^{-4} Hz, which is the smallest value. Taking into consideration that these two islands are located at a long distance of 400 km, it is very interesting that we could find almost the same frequency for the maximum correlation coefficients.

We will consider the significance of the same frequency based on other data. The spectrum averaged for many tide stations located at the coast of Japan is shown in Fig.12, which was obtained for the initial three waves in the Japan Sea Tsunami by Abe and Ishii(1983). The figure shows that the tsunami had a predominant frequency of 1.4×10^{-3} Hz at the initial stage. The predominant one coincides with the one obtained for the most correlative frequency of the Awashima model. This fact suggests that the maximum inundation waves observed at these two islands are the same waves. It is concluded that the waves, which brought the maximum levels and determined the characteristic distribution in the island, were observed at the early stages in many tide stations. In fact we obtained an information that the maximum level at the west coast of the Awashima Island was attained to by the second wave at the survey. It was shown by the tide gage record that the early arrival of the maximum level was not true for the east coast of the Awashima Island. It took about 1 hour from the first arrival to the maximal arrival at the station of Uchiura, which is shown in Fig.13 after reducing the ordinary tide. But the maximum level at the east side did not overcome one at the west side. It was confirmed that the characteristic distribution of the maximum heights along the circumference of the island was determined at the early stage of the tsunami.

In the Okushiri Island no tide gage operated at the time of the Japan Sea Tsunami. It is difficult to discuss the history at this island. But we also have a proof of the early arrival of the maximum inundation wave at the south tip of the island. According to the witness the second wave was the highest. There is a strong possibility that the characteristic distribution of the maximum heights observed at the Okushiri Island was also determined at the early stage.

The predominant frequency was high in coparison with the case of the 1964 Niigata Tsunami(Abe and Ishii,1983). The 1983 Japan Sea Tsunami brought a considerably high wave to the Awashima Island but the 1964 Niigata Tsuanmi never brought such one to the island in spite of a near source(Aida et al., 1964). The difference is attributed to one of the frequencies of the tsunami waves. The high frequency wave functions as a good contributor to high level at the island coast of small scale facing to the incident direction. This fact was verified from the frequency dependence of the amplitude by the nume-

rical computation. The high frequency wave resulted in the characteristic distributions, which shows a high level at the coast of incoming direction and a sharp decrease at the coast of opposite side, observed at the small islands.

The origin of the predominant frequency of 1.4×10^{-3} Hz was discussed by Abe and Ishii(1983). They explained that the frequency was determined by a fundamental relation of wave between wave length and velocity, which is reduced to the sea depth of the source, and obtained the frequency of 1.4×10^{-3} Hz for the length and sea depth of 110 km and 2500 m, respectively. The source was obtained by Hatori(1983) and the fault models were refined on the standpoint of tsunami generation by Aida(1984) and Satake(1985). The length of 110 km is a linear dimension of the model fault. Thus the predominant frequency was explained by them as the direct wave from the source. The frequency is in proportion to the square root of the sea depth of the source and reverse proportion to the source length. The high frequency wave was excited in spite of a large length of the source area in the 1983 Japan Sea Tsunami. Thus it is nessary to point out the role of the intermediate sea depth of tsunami source. The characteristic distribution of the maximum heights observed at the small islands is related to the intermediate sea depth. The fact is useful to predict a high elevation of water level at a small island by the tsunami of deep sea origin.

A spectrum was computed for the tide gage record observed at the east side of the Awashima Island and was shown in Fig.13 with the time history of the tsunami. The spectrum was computed for 12 hours from the origin time of the earthquake with the sampling interval of 1 min. The predominant frequency of 0.75×10^{-3} Hz explains a development of the wave at the east side of the island. The wave profile suggests an excitation of natural oscillation of fundamental mode between the island and the Honshu Island as shown in Fig.14. The fact that the maximum level was attained to by the 7th wave at the east coast and the inter-island oscillation was observed proves a contribution of the Honshu Island to the maximum level at the east side.

Discussion

Sakai(1984) also investigated a topographic effect of the Okushiri Island on the basis of the time historical computation for the sinusoidal wave and showed a similarity of wave energy concentration observed at the south tip to the result from the amplitude computation for the period of 8-10 min. He used the period ranging from 5 to 10 min at the interval of 1 min. His result showed a tendency that the wave concentrated to the south tip with increase of the period. Taking into consideration that the maximum period which he used is 10 min(1.67×10^{-3} Hz), we can find a consistency of our result to his one.

We could not observe a remarkable peak at the frequency component of 1.4×10^{-3} Hz in the spectrum observed at Uchiura in the Awashima Island, which was regarded as one of the incident wave. The fact is attributed to the formation of a shadow zone to the wave incident from the outer sea to the east side. A simple calculation of wave length shows 21 km in length

from assuming the shelf depth of 90 m and the frequency of 1.4×10^{-3} Hz. The linear dimension of the island occupies one third of the wave length and is long enough to prevent from propagating. The time history observed at Uchiura explains as shown in Fig.13 that the wave having a lower frequency arrived as the initial one.

The Okushiri Island is located on the shelf slope facing to the open sea of intermediate sea depth of 3000 m. On the other hand the Awashima Island is located on the continental shelf of shallow depth of 90 m. It is considered that the sea bottom topography around the island had an important effect on the elevation and distribution of the maximum levels by the tsunami. For the maximum correlation coefficient the Awashima Island had the value larger than that of the Okushiri Island. This fact implies a superiority of the model for the Awashima Island. The small lowering of the maximum correlation coefficient in the Okushiri model is considered to be a result of large difference between computed amplitude and observed one at the south east coast. One of the reasons causing the difference is a plane wave approximation for the incident wave. The Okushiri Island has a long spur extending toward the south. Such a topography has a possibility of distorting the plane wave condition.

Finally it is significant to add a comment to the small difference of the best fitting frequencies between two models. As described before the frequencies were 1.4×10^{-3} Hz for the Awashima model and 1.5×10^{-3} Hz for the Okushiri model. The islands are located on the opposite direction from the source area. It was shown by Shimazaki and Mori(1985) that the earthquake resulted from a superposition of elastic waves generated on two fault planes, which were a bit separated in the N-S direction. According to them the south fault was generated in the first time and the north one followed. We approximate the destructive motion on the two fault planes as a continuously moving rupture from the south margin to the north one. Generally a moving source of wave is known as a cause of Doppler effect. Assuming that the interval of two pulses generated at the instances of the start and stop of fault formation controls a wave period, we can expect the period or frequency to differ in the propagation direction from the Doppler effect. The shift of frequency to high side is observed in the coming direction and and it to low side is observed in the leaving direction. When take into consideration of the south location of the Awashima Island for the source and the north one of the Okushiri Island, the trend of frequency shift is consistent to the idea. In the assumption of continuous propagation from south to north with the rupture velocity of v, the ratio of the frequency f_n observed at the north observation point to that of the south one f_s is obtained to be

$$\frac{f_n}{f_s} = \frac{v + c}{v - c}$$

in which c is a long wave velocity. When we take the sea depth of 2000 m and the rupture velocity of 3 km/s, the frequency ratio of 1.1 is expected. This value is an approximation of the frequency ratio for the maximum correlation frequency at the Okushiri Island to that at the Awashima Island. This estimation supports our consideration for the small difference between two maximum correlation frequencies obtained at the two islands.

Conclusion

We investigated the harmonic response of long wave to two small islands to explain the characteristic distribution of the maximum inundation heights observed in the 1983 Japan Sea Tsunami. The amplitude distribution was computed for the area including the island and the coast of the Honshu Island in Japan by the use of sinusoidal plane wave of frequencies ranging from 1.0×10^{-4} to $20. \times 10^{-4}$ Hz. The observed heights were compared with the computed ones for each frequency in each island and the correlation coefficients were estimated to identify the best fitting frequency. As the result it was found that the observations were explained by the frequencies of 1.4×10^{-3} Hz and 1.5×10^{-3} Hz for the Awashima Island and the Okushiri Island, respectively. Since these two values are nearly equal and coincided to the predominant frequency observed by many tide gages for the initial three waves, it was concluded that these two waves contributing to the maximum correlation were attributed to the direct wave from the source.

Acknowledgement

The author expresses an acknowledgement to Professor Murata and Mr. Yamashita for the discussion and is indebted in computation to the Computer Center of the Tokyo University.

References

1. Abe, Kuniaki and Ishii, H., "Tsunami Source of Nihonkai-Chubu Earthquake," Abstr. Seismol. Soc. Japan, No.2, pp.36(1983),(in Japanese).

2. Aida, I., "A Source Model of the Tsunami Accompanying the 1983 Nihonkai-Chubu Earthquake," Bull. Earthq. Res. Isnt., Tokyo Univ., Vol.59, pp.93-104 (1984) (in Japanese).

3. Aida, I., Kajiura, K., Hatori, T. and Momoi, T., "A Tsunami Accompanying the Niigata Earthquake of June 16, 1964," Bull. Earthq. Res. Inst., Tokyo Univ., Vol.42, pp.741-780 (1964) (in Japanese).

4. Hatori, T., "Tsunami Magnitude and Source Area of the Nihonkai-Chubu (the Japan Sea) Earthquake in 1983," Bull. Earthq. Res. Inst., Tokyo Univ., Vol. 58, pp.723-734 (1983) (in Japanese).

5. Honma, S., "On the Behaviour of Seismic Sea Waves around Circular Island," Geophys. Mag., Centr. Meteol. Obs., Vol.21, pp.199-208 (1950).

6. Houston, J.R., "Interraction of Tsunamis with the Hawaiian Islands Calculated by a Finite-element Numerical Model," Jour. Physical Oceanography, Vol.8, pp.93-102 (1978).

7. Kawahara, M., Takeuchi, N., and Yoshida, T., "Two Step Explicit Finite Element Method for Tsunami Wave Propagation Analysis," International Jour. Numerical Methods in Engineering, Vol.12, pp.331-351 (1978).

8. Sakai, T., "Tsunami Behaviour around the Island," Res. Rep. Tsunami Disastor Prevention Labo., Faculty of Technology, Tohoku Univ., Vol.1, pp.63-77 (1984) (in Japanese).

9. Satake, K., "The Mechanism of the 1983 Japan Sea Earthquake as Inferred from Long-period Surface Waves and Tsunamis," Phys. Earth Planet. Interiors, Vol.37, pp.249-260 (1985).

10. Shimazaki, K., and Mori, J., "Focal Mechanism of the May 26, 1983 Japan Sea Earthquake," Abstr. Seismol. Soc. Japan, No.2, pp.15 (1983) (in Japanese).

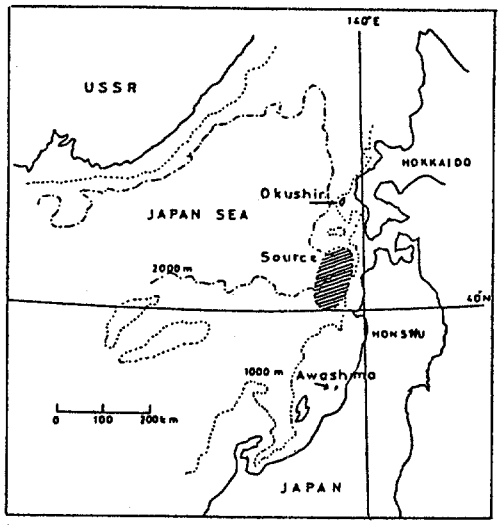

Fig.1

Fig.1. Locations of the Okushiri and Awashima Islands with source area derived by Hatori(1983).

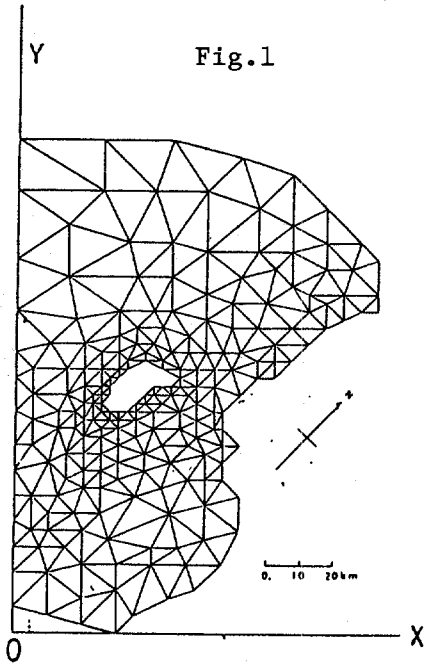

Fig.2

Fig.2. Finite element grid for the Okushiri Island.

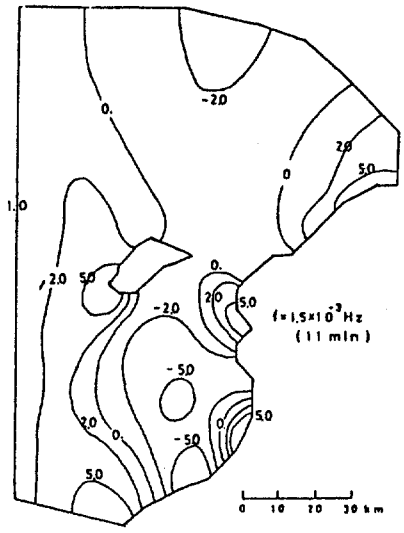

Fig.3

Fig.3. Amplitude distribution computed for frequency of 1.5x10 Hz.

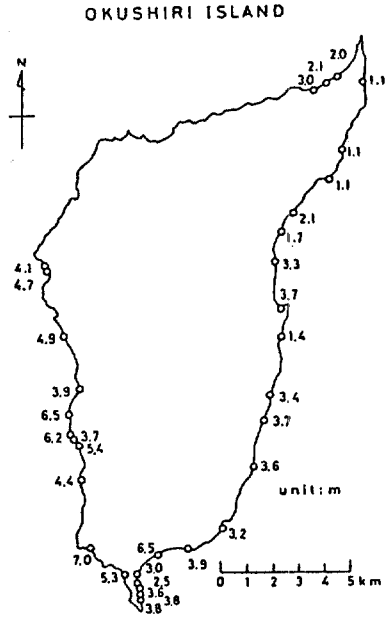

Fig.4

Fig.4. Maximum inundation heights above mean sea level observed in the Okushiri Island(Abe and Ishii,1983).

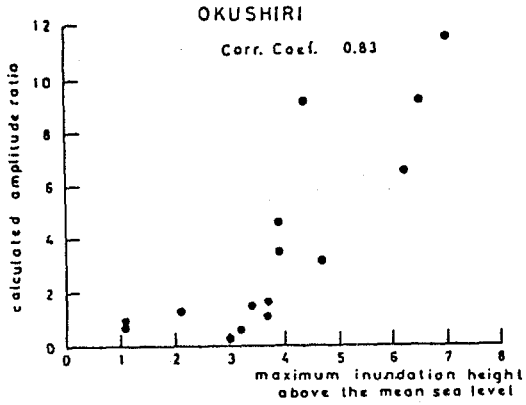

Fig.5. Correlation diagram between observations and computations for frequency of 1.5x10 Hz.

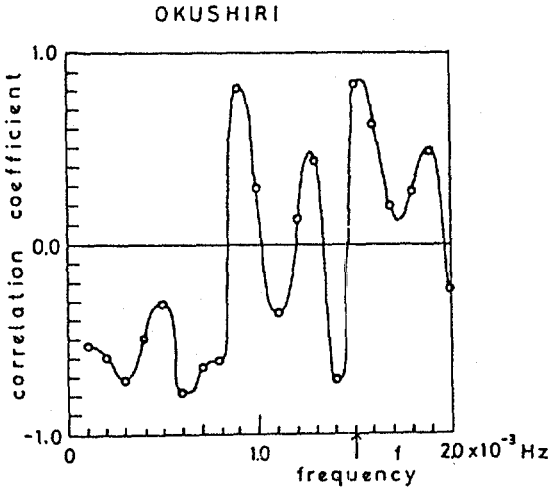

Fig.6. Frequency dependence of correlation coefficient in the Okushiri Island. The most correlative frequency is indicated by an arrow.

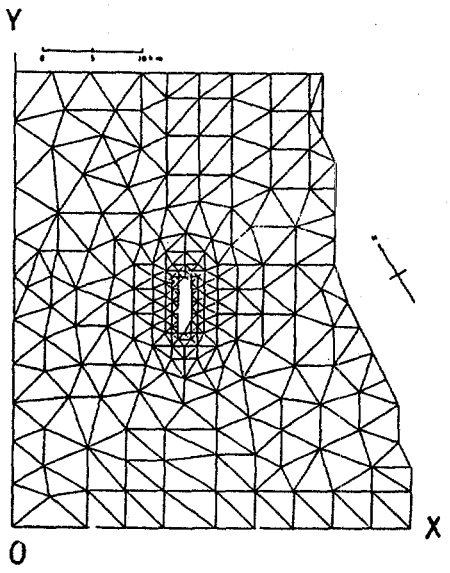

Fig.7. Finite element grid for the Awashima Island.

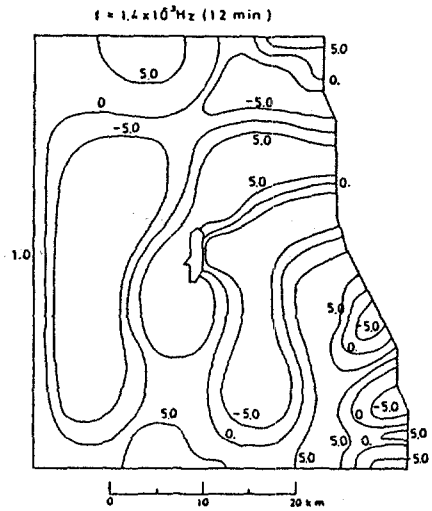

Fig.8

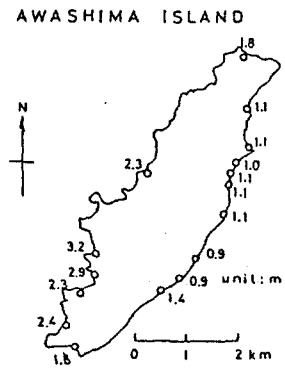

Fig.9

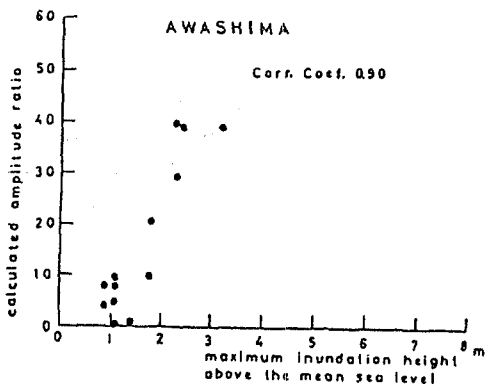

Fig.10

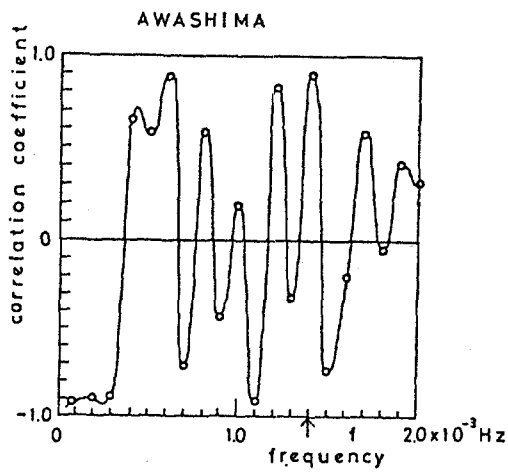

Fig.11

Fig. 8. Amplitude distribution computed for frequency of 1.4x10 Hz.

Fig. 9. Maximum inundation heights above above mean sea level observed in the Awashima Island(Abe and Ishii, 1983).

Fig.10. Correlation diagram between observation and computation for frequency of 1.4x10 Hz.

Fig.11. Frequency dependence of correlation coefficient in the Awashima Island. The most correlative frequency is indicated by an arrow.

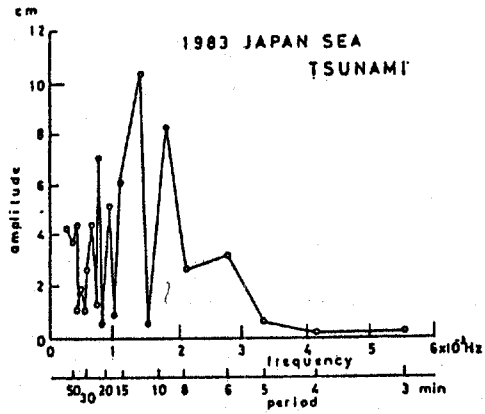

Fig.12. Average spectrum for first three waves observed by many tide stations located along Japan Sea Coast in the 1983 Japan Sea Tsunami(Abe and Ishii, 1983).

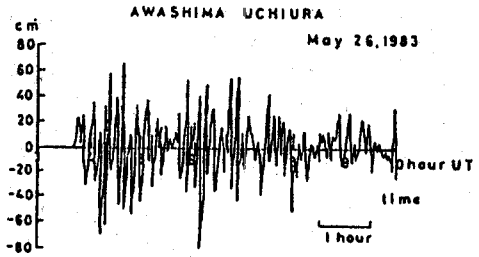

(A)

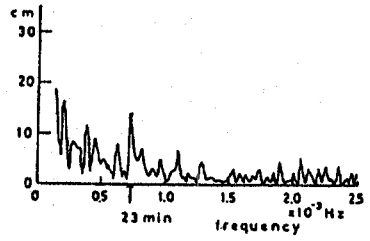

(B)

Fig.13. Time history of tsunami obtained at Uchiura located at east side of the Awashima Island(A) and amplitude spectrum of above time history for 12 hours from earthquake origin time of 3h 00m UT(B).

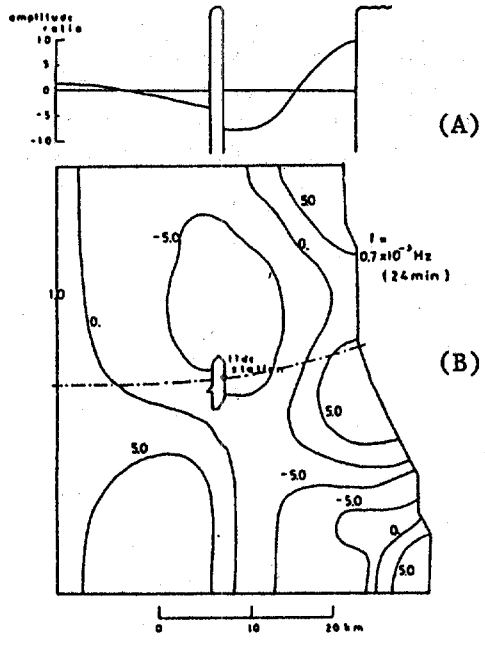

Fig.14. Amplitude distribution(B) and the profile along chain line computed for frequency of 7.0x10 Hz(A).

EFFECTS OF BATHYMETRIC ROUGHNESS UPON TSUNAMI TRAVEL TIME

GREG HOLLOWAY, TAD MURTY, AND EDMAND FOK
INSTITUTE OF OCEAN SCIENCES
P.O. BOX 6000
SIDNEY, B.C.
V8L 4B2

ABSTRACT

We examine the effect of unresolved bathymetric variations ("roughness") upon the calculation of tsunami travel time. From approximately 40,000 km of high quality trackline data in the abyssal North Pacific, we obtain systematic corrections in the sense of increased travel time. Non-Gaussian statistics of the bathymetry are seen to be significant. An empirical correction is suggested to facilitate incorporation of roughness statistics into operational tsunami warning charts. This correction amounts to at most a few minutes over several hours of travel.

1. INTRODUCTION

Tsunami travel time charts in operational use by warning centers are based upon bathymetric data largely obtained prior to 1948. A good deal of high resolution bathymetry has since become available. However, trackline bathymetry is not directly useful for travel time chart preparation which requires two-dimensional coverage. Therefore most bathymetric detail is omitted. For convenience we refer to all omitted detail as "roughness"; retained bathymetry as "smoothed". The question that we address is how to use statistics from high resolution trackline to obtain systematic corrections to travel time charts based on smoothed bathymetry.

Concern in this note is limited to effects of abyssal roughness on the suppositions (a) that detailed bathymetry is usually available on continental margins and (b) that travel time calculations are more sensitive to bathymetric detail on continental margins, hence warranting greater effort. For the North Pacific we have defined "abyssal" as lying seaward of the most inshore 5 km isobath. (Crossing the Japan Trench we elect to define abyssal from the 5 km isobath lying seaward of the trench axis.)

We have extracted approximately 40,000 km of high quality trackline from data archived by the NOAA National Geophysical and Solar-Terrestrial Data Center, involving records from the ships Melville and Oceanographer. A composite of the trackline portions is shown in Fig. 1. Absyssal portions, as defined, were identified and concatenated in the order indicated on Fig. 1. Occasional but rare data gaps were removed by cutting such portions then splicing to a nearly equal depth across the gap. The result was to obtain a "synthetic trackline" of length 39,452 km along which depths were linearly interpolated at a uniform spacing of 2.4 km. The composite depth trace is shown in Fig. 2a.

Of course the depth trace in Fig. 2a is not that which would underlie any actual tsunami trajectory. Rather, we have constructed this record as a collection of actual abyssal roughness, here representative of portions of the North Pacific basin. It should also be remarked that we have no information concerning horizontal anisotropy of roughness which we therefore ignore.

2. THE MATHEMATICAL PROBLEM

With bathymetric resolution at 2.4 km spacing, we are including scales small compared with tsunami wavelengths. Dynamics of shallow water wave interaction with bathymetric variation may lead to amplitude and frequency dispersion. However we neglect this interaction and consider that isophase surfaces $\Phi(\underline{x},t) = \Phi$, propagate at local phase speed $(gh\ (x))^{\frac{1}{2}}$ where $h(\underline{x})$ is the local depth of a resting fluid. The bathymetric variance spectrum is sufficiently "red" that influences of fluctuations on short length scales are slight. For convenience we treat all scales uniformly when defining travel time from x_1 to x_2

$$\tau_{12} = \int_{x_1}^{x_2} (gh)^{-\frac{1}{2}}\, dx \qquad (1)$$

where g is acceleration due to gravity.

The question is, if $h(\underline{x})$ is only resolved to some coarse scale, how does

τ depend upon that resolution scale? Moreover, we seek a correction to take account of unresolved roughness.

To examine this, we produce a coarsely resolved or smoothed bathymetry by low pass filtering the record in Fig. 2a under a Gaussian Fourier filter

$$F(k) = e^{-k^2 s^2/2} \tag{2}$$

where k is wavenumber and s is a smoothing length scale. Examples of smoothed bathymetry are shown in Fig. 2, traces b - e, for successively larger s.

The solid curve in Fig. 3 shows the increase in calculated τ as resolution is refined, i.e. s made smaller. A referance travel time τ_o is based solely upon mean depth

$$\bar{h} = (x_2 - x_1)^{-1} \int_{x_1}^{x_2} h \, dx \tag{3}$$

Increasing τ with decreasing s is readily understood. Define dimensionless elevation $\varepsilon(x_j s)$ as

$$h(x;s) = \bar{h}(1 - \varepsilon(x_j s)) \tag{4}$$

where h(x;s) is bathymetry smoothed to scale s. Relative travel time τ/τ_o is

$$\tau/\tau_o = \overline{(1 - \varepsilon)^{-\frac{1}{2}}} \tag{5}$$

where overbar denotes x-averaging as in (3). Binomial expansion from (5) then yields

$$\tau/\tau_o \approx 1 + \frac{3}{8}\overline{\varepsilon^2} + \frac{5}{16}\overline{\varepsilon^3} + \frac{35}{128}\overline{\varepsilon^4} \tag{6}$$

plus terms of order $\overline{\varepsilon^5}$ and higher.

The approximation to τ/τ_o through terms retained in (6) is evaluated for a sequence of values of s and shown as a dashed curve in Fig. 3. Effects of terms of order higher than $\overline{\varepsilon^4}$ are only apparent for very small s.

It is interesting to compare results if one assumes Gaussian statistics for ε, hence $\overline{\varepsilon^3} = 0$ and $\overline{\varepsilon^4} = 3\,\overline{\varepsilon^2}^2$, i.e.

$$\tau/\tau_o \approx 1 + \frac{3}{8}\overline{\varepsilon^2} + \frac{105}{128}\overline{\varepsilon^2}^2 \tag{7}$$

This Gaussian assumption is also plotted as a dash-dot curve in Fig. 3. The systematic effect of non-Gaussianity is apparent, both on account of skewness $\overline{\varepsilon^3} > 0$ that may be seen in Fig. 2 and on account of kurtosis $\overline{\varepsilon^4}$

greater than 3 $\overline{\varepsilon^2}^2$.

As a practical consideration, higher statistics $\overline{\varepsilon^3}$ or $\overline{\varepsilon^4}$ are poorly known for oceanic bathymetry whereas $\overline{\varepsilon^2}$ can reasonably be estimated for given s. Therefore one may wish to approximate τ/τ_o by an expression such as (7), involving only $\overline{\varepsilon^2}$. A relatively simple "curve fit" which preserves a $1 + \frac{3}{8}\overline{\varepsilon^2}$ at small $\overline{\varepsilon^2}$ and which approximates the solid curve in Fig. 3 may be given by

$$\tau/\tau_o \approx (1 + \frac{3}{8}\overline{\varepsilon^2} + \frac{105}{128}\overline{\varepsilon^2}^2)^{1+\gamma\overline{\varepsilon^2}^2} \qquad (8)$$

with $\gamma \approx 1500$ from the bathymetry here examined.

In reality, bathymetric roughness is not statistically homogeneously distributed. Operationally, one envisions calculating τ from a sum of segments characterized by local $\bar{h}$ and by local $\overline{\varepsilon^2}$, utilizing an expression such as (8) to correct τ for local $\overline{\varepsilon^2}$. The procedure is facilitated by defining for each segment an "effective mean" depth

$$\bar{h}_{eff} = \bar{h}(\tau_o/\tau)^2 \qquad (9)$$

where τ/τ_o might be from (8) or, perhaps, simply as $1 + \frac{3}{8}\overline{\varepsilon^2}$. It is seen that $\bar{h}_{eff}$ is systematically shallower than $\bar{h}$.

3. OPERATIONAL TSUNAMI WARNING CHARTS

The tsunami travel-time charts that are being used operationally in the tsunami warning system for the Pacific Ocean were constructed originally by the U.S. Coast and Geodetic Survey in 1948, following the disastrous Aleutian earthquake tsunami of April 1, 1946. Making use of the bathymetric data available till the mid-1940's, and employing ray tracing techniques, travel times for the leading wave of the tsunami were computed from the Green-Du Boys formula, which is generally used for determining the phase speed of long gravity waves such as tsunamis.

$$c = \sqrt{gh}$$

The travel time between any two locations was then calculated using equation (1). In the above equation, c is the phase speed, h is the average depth between two given points and g is acceleration due to gravity. Zetler (1947) described the details on the construction of the charts. The U.S. National Ocean Survey (Anon., 1971) revised these charts and presented travel time contours for fifty gauge locations around the Pacific Rim. It is generally claimed that these charts are accurate to within ±1.5 minutes for each hour of tsunami travel (Murty, 1977).

Murty (1986) showed that the above claim is not justified in several cases and substantial errors exist in these charts (also see Saxena, 1977). At least discrepancies may be attributable to the rather poor quality of the bathymetric data available in the 1940's for the Pacific Ocean. There are also inaccuracies in the determination of the exact travel time of a tsunami to a given tide gauge station.

It would be highly desirable to compare our results with some observed tsunami travel times. Unfortunately this cannot be done at this time, because the operational tsunami travel time charts are not sufficiently accurate for this purpose. Also, the travel path of any tsunami will not coincide with any of the tracks shown in Fig.1. It should be noted that the correction proposed here is rather small and may amount at most to a few minutes.

At present the predicted travel times are generally greater than the observed travel times, and this study shows that, including the bottom roughness will increase this difference by a few minutes more.

One of the reviewers pointed out that it is better to have the predicted travel times greater than the observed travel times because in the opposite situation where the predicted travel times are less than the observed times, the public will treat it as a false alarm and return to the scene. Thus the small correction due to bottom roughness is on the conservative or safer side.

With the improvement of hydrographic techniques for ocean depth soundings, there is a good possibility that the bathymetric charts will be sufficiently accurate so that travel-time differences with and without the inclusion of bottom roughness could be identifiable.

Another referee suggested that effects of bottom roughness should be ascertained, by averaging the bathymetric data first in $5^\circ \times 5^\circ$ latitude-longitude grids, then $2.5^\circ \times 2.5^\circ$, and even smaller grids. When more accurate bathymetric charts are available, this type of calculation would be meaningful.

ACKNOWLEDGEMENTS

We thank Roopa Ghosh for typing the manuscript and Rosalie Rutka for drafting the diagrams.

REFERENCES

1. Anon. 1971. Tsunami Travel Time Charts, for Use in the Tsunami Warning System, National Ocean Survey, Rockville, MD, U.S.A., June 1971, 53 pp.

2. Murty, T.S. 1977. Seismic Sea Waves - Tsunamis. Bull, 198, Fisheries Res. Bd. Canada, Ottawa, 337 pp.

3. Murty, T.S. 1986 Tsunami Travel Time charts: A Critical Look at Ocean Depth Data, In Proceedings of PACON-86, Honolulu, March 23-27, 1986 (in press).

4. Saxena, N.K. 1977. Improvement of Tsunami Prediction by Marine Geodetic Techniques, Proc, IUGG Tsunami Symp, Ensenada, Mexico, Report No. 48, Marine Environmental Data Service, Ottawa, 245-246.

5. Zetler, B.D. 1947. Travel Times of Seismic Sea Waves to Honolulu. Pacific Science, Vol. 1, No. 3, 185-188.

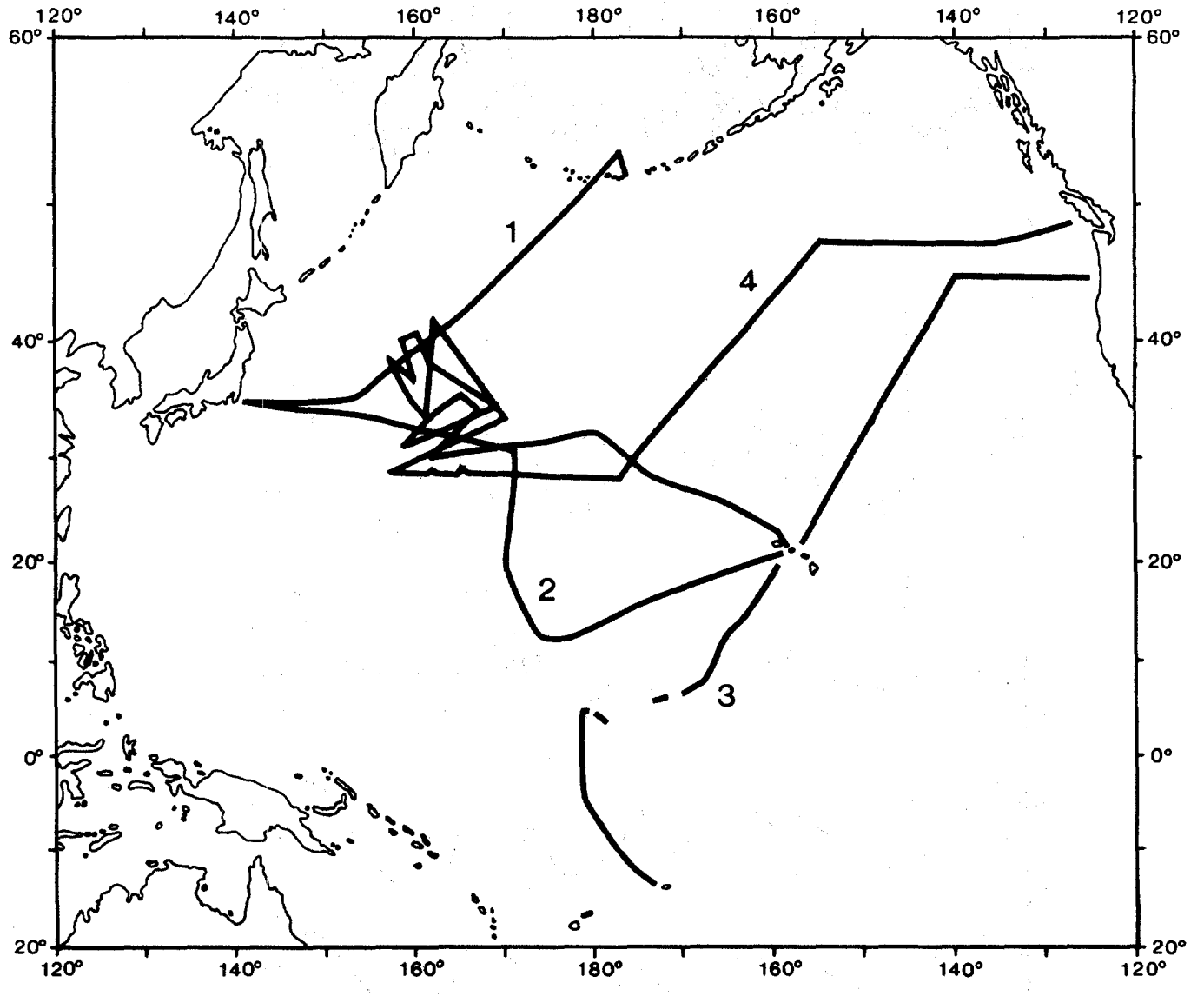

Fig. 1 Tracklines of ships Melville (legs 1, 2, 3) and Oceanographer (leg 4) are shown.

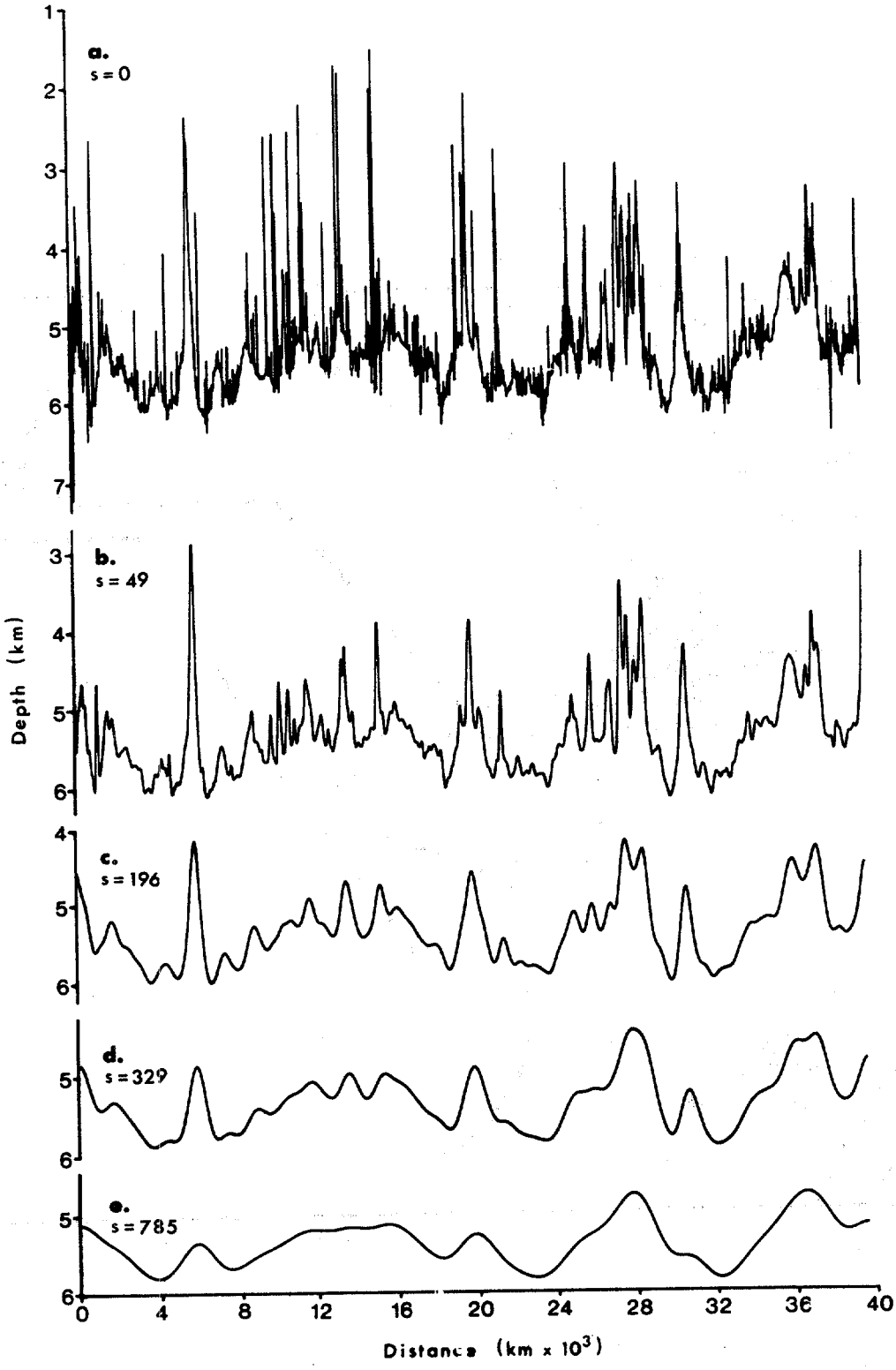

Fig. 2 A synthetic bathymetry from the sequence of tracklines in Fig. 1, with data gaps removed, is shown in Fig. 2a. The bathymetry is then smoothed under a Gaussian Fourier filter and shown in traces b, c, d, and e for smoothing scales of 49, 196, 392, and 785 km, respectively.

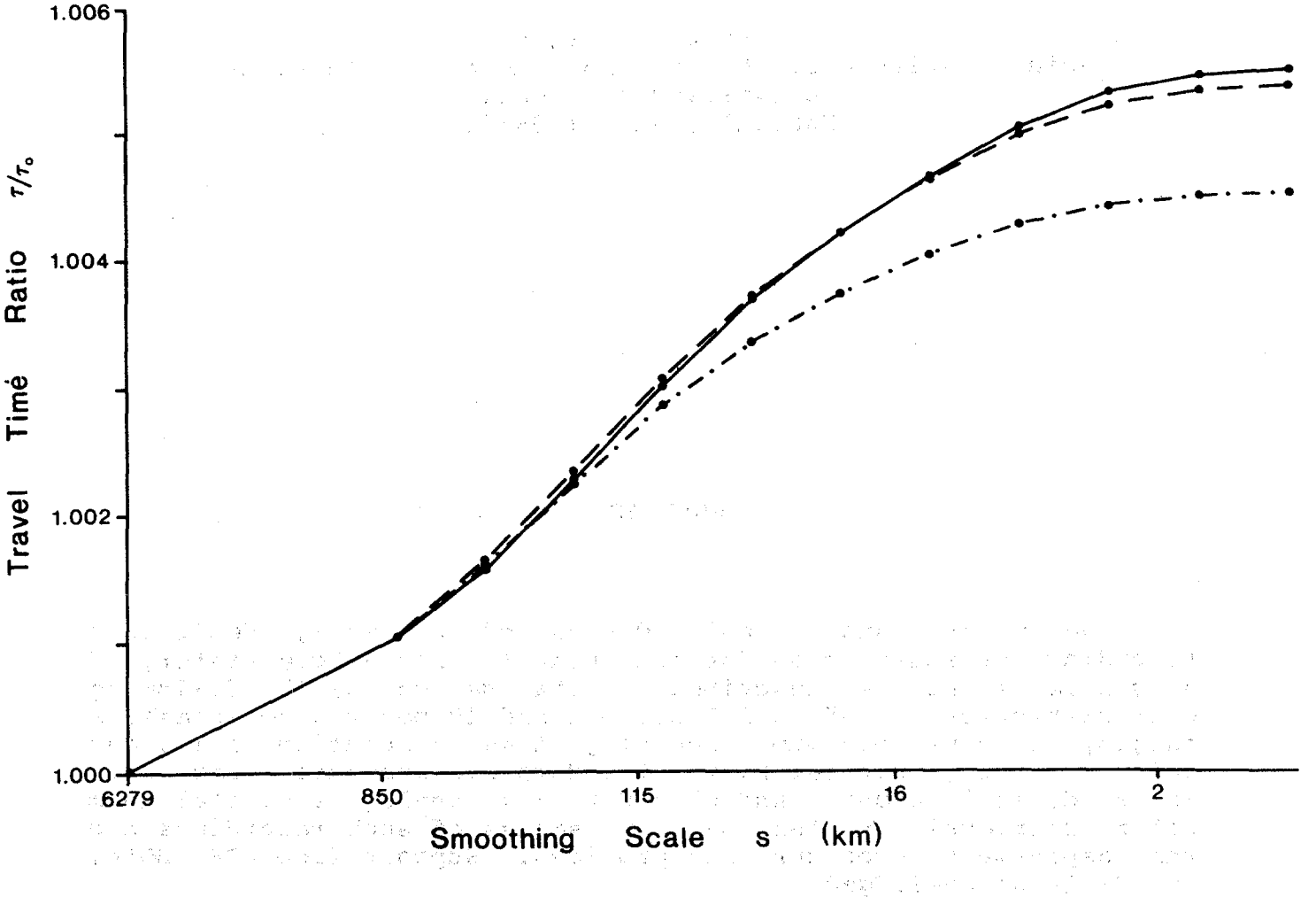

Fig. 3 The ratio of calculated travel time τ to travel time based upon mean depth alone is shown. As smoothing scale s is reduced so that more bathymetric roughness is retained, calculated travel time (solid curve) increases. An approximation based on assumed Gaussian probability of bathymetric fluctuation is shown (dash-dot curve). A further approximation including non-Gaussian third and fourth moments is also shown (dashed curve).

Design and Development of a Coastal Tsunami Gage

George D. Curtis
Joint Institute for Marine and Atmospheric Research,
University of Hawaii,
Honolulu, Hawaii 96822

ABSTRACT

Development and final design of a small, deployable recording pressure gage for obtaining the near-shore history of a single event is described. The device has the following characteristics: 4" x 12" size; 1 and 10 meter water-pressure ranges; 12-hour minimum recording time, resolution of 1%, and 100% over-range without harm. The data are recorded permanently in a digital memory and played back in analog or digital form after retrieval of the gage. Examples of such recordings and the deployment procedure are provided. Support from NSF, NOAA, and UH is acknowledged.

BACKGROUND

In the late 70's, JIMAR developed and built several analog pressure gages for deployment upon warning of a tsunami. Because of their mechanical nature, packaging, and other problems, they were not replicated and put into use.

It was felt that a device with no moving parts, properly packaged and powered, would resolve these problems and was possible with digital integrated circuitry. Such a system was designed and a paper describing it presented at a tsunami conference (ref. 1). That paper summarized the development as follows:

"A relatively inexpensive device which will record the water level time-history in a coastal location during a tsunami event is approximately 2 cm by 20 cm and is secured at a pre-selected site in shallow water when a tsunami is enroute. The recording system includes a semiconductor pressure sensor, analog-to-digital conversion, a clock, a semiconductor memory for data storage, and batteries. Tentative specifications are: 1 and 10 meter ranges; 0.5% (of full range) resolution; 30 second sampling interval, and storage for 10 hours of data. Upon retrieval after the event, the unit is opened in the lab and the stored data read out onto a chart recorder to produce a conventional-appearing tide-gage record, or used directly for computer analyses. Trade-offs in design parameters, cost, electronic and physical characteristics, and deployment factors are analyzed."

Fig. 1 is a block diagram of the proposed gage. Subsequently, the important concept of "burning" the data into an electrically programmable read-only memory (EPROM) rather than writing it into the random access memory (RAM) was developed. It was considered novel and a patent was applied for (no. 06/213,940). This was not pursued when it was found that in face of an earlier patent assigned to the Navy only a few claims could be granted; those features are now in public domain. However, the patent work was helpful in advancing the design and in generating a proposal to the NSF. (Prior work had been supported at a modest level by NOAA and UH). A grant was received from NSF for "Improvements in Collection and Dissemination of Tsunami Data" which included the task of developing a prototype gage.

GAGE DEVELOPMENT

With the aid of a subcontract to a local specialty computer company, breadboard and laboratory test versions of the digital portion of the gage were designed and operated.

The analog portion was similar to the old gage. The basic modifications were: a) inclusion of more low-pass filtering to avoid aliasing in the digital system; b) use of two fixed-gain settings, to permit simple deployment; and c) use of a Foxboro transducer-amplifier as an alternate to the National Semiconductor device. The filter parameters desired are

depicted in figure 2, from ref. 1. The implementation of the analog portion was done by two senior EE students, and subsequently by a part-time technician; while educational values resulted, progress was not rapid nor always optimum.

The digital portions included an analog-to-digital (A-D) converter, a clock, and a data storage system. The converter is a low speed, 8 bit system, chosen because it is common in similar devices and provides adequate resolution - 1 part in 256; better than the 1% accuracy of the transducer.

For the data storage system, the advantages of "burning" the "data words" - actually three digit numbers - into an EPROM were decisive and this was the method implemented.

A breadboard was used for program development and as a playback means for prototype tests. A prototype, with a pressure case, was also assembled. It was later reduced in size and used in tests with simulated waves in our Ocean Engineering Laboratory. A large battery provided for long duration testing. Fig. 3 shows some results from the tests in the lab.

Redesign of the electronics for a field prototype (4") resulted in a lower current drain, which permitted the use of penlight cells. Additional energy savings were realized with reduced duty cycle circuitry to match the one sample per minute required to exceed the Nyquist criterion for the actual tsunami recorder, which is intended to operate 12 hours.

Finally, a commercial product appeared on the market which could substitute for much of the digital electronic system. This device is the Datapod 113 made by Omnidata International. (The system bears no patent notice). Such developments are both inevitable and desirable in fast moving fields of technology.

FINALIZED VERSION

Ref. 2 was a final report on the entire project to the NSF, detailing the development and uses, and providing recommendations on a finalized version for trial deployment. Although no outside funding appeared, the University of Hawaii responded to a brief proposal with research funds to fabricate five units of an interim version. This version was then designed with the following characteristics and goals:

* "Slow" sample rate (1 per minute exceeds the Nyquist criterion).
* Simplified circuitry; more compact and with reduced battery drain.
* Smaller, sealed case, similar to the original mockup.
* Permanent lithium batteries (5-year minimum storage life).

* Magnetic switches, without case penetration; range selection, with default to 10 meter range.

* Use of off-the-shelf components insofar as possible.

The design met these goals with minor exceptions, discussed later. Fig. 4 is a block diagram of the system; fig. 5 is a photo in a test deployment.

The input port, exposed to ocean pressure directly or via a tube, leads through a filter to the pressure transducer. The filter, of sintered polyethelyne or silicone oil-saturated silica, provides a barrier against sea water and helps prevent artifacts from wave slap, etc. The pressure transducer is a piezo-resistive strain gage which incorporates an integral amplifier and has a range of 0-15 PSIG (10 meters H_2O); it is not harmed by twice that pressure. The analog output is set for 1 meter of water full scale of the recording system, and divided by 10 with a resistor network to obtain the 10 meter range, controlled by a magnetic reed switch for 1 or 10 m range. The signal is then inputted to the modified Datapod 113, which samples it periodically and records the levels in a 2K EPROM. At the 1 per minute rate, the system can provide up to 17 hours of water level (i.e. pressure) history.

To provide both adequate shelf life and at least 12 hours recording life, lithium cells are substituted for the alkaline cells normally used in the Datapod. Since lithium cells are 3 volts each, the battery cases are rewired to provide 12 volts from each half-section to the Datapod, and to the transducer and other external needs separately. These include a LED pilot light which assures the operator the system is functioning and a time-delay relay which handles a software problem. Turn-on utilizes a reed switch held open by an external magnet taped in place; the magnet is simply removed to activate the device. The magnet can then be placed in a slot to operate the other reed switch if the high sensitivity range (1 meter) is desired. (Defaults are ON and 10 m).

A useful feature of the Datapod, which is apparent in spite of its ineptly written manual, is the ability to change the recording interval by internal switches so that tides and other long term data can be recorded (this was used in most tests).

To "play-back" the recorded data, the EPROM is removed from the Datapod and placed in our breadboard system and the D-A converter is output to a strip chart recorder, as was done for fig. 3. Alternatively, the EPROM can be read with a decoder (supplied by Omnidata) and a computer terminal. The resulting numerical data are read from the screen, printed, or used in analyses. After file storage of the data, the EPROM can be erased by exposure to an ultraviolet lamp, and re-used.

RESULTS AND RECOMMENDATIONS

Since the tidal range in Hawaii is usually less than a meter, it is convenient to test the gage on the 1-meter range (and tide can be used as a calibration in an actual tsunami). Fig. 5a shows the analog recording from a portion of a tide cycle, with the numerical output listed in 5b. This was produced with the first of five gages being fabricated in the University lab. Note that the gage was actually on the 10m range in this test.

After testing, the five devices are being distributed to a nucleus of volunteer observers (ref. 3), to await a mini-tsunami (ref. 4). An early application was to record wave action from the Aleutian earthquake of May 17, 1986. There was moderate action at the locations used on Oahu; the trial did help uncover problems with the device and its deployment, but produced some data.

The selected sites will either have a shallow water point (piling, etc.) to which the gage can be secured (it is slightly positively buoyant) or an on-shore location at which the gage can be connected to a tube leading to the ocean (Appendix A gives site criteria). Upon a tsunami warming, the observer turns the system on, verifies operation by the flashing pilot-light (it flashes instead of lighting continuously to conserve battery energy but is quite noticeable) and notes the start time. He then sets the range, affixes the gage, and departs for a safe area, if appropriate. The device can be retrieved and the EPROM removed at any time; the data will not over-write, nor be lost when the battery runs down. The O-ring sealed case can then be opened, the EPROM and batteries replaced, and the gage returned to service. If the operator finds a problem such as prior activation when preparing to deploy the gage, he can replace these parts if spares are available at his location.

Final deployment and field tests by volunteer observers are the only way to verify the design and useability of this gage. The need (ref. 5) and applications (ref. 1) have been previously shown; this was recently emphasized in ref. 6. After evaluation, funding will be sought for a "productized" version, expected to be smaller and cheaper (aluminum case, custom version of the Datapod, etc.). Although tentative deployment sites have been selected in the Hawaiian Islands, Alaska, the U.S./Canada West Coast, Japan and the USSR are potentially productive areas for their use. The real goal is to deploy enough reasonally-priced instruments in selected locations so that with a fair percent recovery of data from even small ("research") tsunamis, a significant advance in hazard mitigation and quantitative warming can be made.

ACKNOWLEDGMENTS

Support from the University of Hawaii Research Fund and from the Joint Institute for Marine and Atmospheric Research is gratefully acknowledged. This is JIMAR Contribution No. 86-0118. An earlier version of this paper was presented at the Pacific Congress on Marine Technology, April 1986, and distributed in the Conference Proceedings.

REFERENCES

1. Curtis, George D. and Loomis, Hal G.: "A Small, Self-Contained Water Level Recorder for Tsunamis," (with H.G. Loomis), IUGG-1979, Canberra, (published 1983). JIMAR contribution 79-0023.

2. Curtis, George D.: Final Report to the NSF, "Improvements in Collection and Dissemination of Tsunami Data", Joint Institute for Marine and Atmospheric Research, University of Hawaii, 1982.

3. Curtis, George D.: "Establishment and Operation of a Tsunami Monitoring Program," Natural Sciences of Hazards, The Journal of the Tsunami Society, October, 1982.

4. Adams, William M., and Nakashizuka, N.: "A Working Vocabulary for Tsunami Study," Science of Tsunami Hazards, the Journal of the Tsunami Society, Vol. 3, No.1, 1985.

5. Bernard, Eddie, and Goulet, Richard: Tsunami Research Opportunities, NSF/NOAA, Washington, D.C., 1981.

6. Van Dorn, William: "New Tsunami Recorder at Wake Island," Journal of the Tsunami Society, Vol. 4, No. 1, 1986.

APPENDIX A

Deployable Tsunami Gages - Hawaii Site and Support Criteria
(by tentative priority)

1. Area - General

   a) Oahu - all coasts

   b) Other high density/high impact areas
      1. Present occupancy/use
      2. Future occupancy/use
      3. People problem first; structure next

   c) Significant tsunami history but:
      1. More data needed; island, orientation, etc.
      2. Other criteria met satisfactorily

2. Specific Site(s)

   a) Provide useful data by a time history (vice max. water level)

   b) Spectral contamination acceptable but:

   c) "Generic" data for the exposure is preferred

   d) Wave action preferred over flooding

   e) Secure, accessible, shallow location preferred; edge of bay, etc.

   f) Installation and operational capability available (see below)

3. Installation and Support

   a) Device can be secured firmly to shore structure and attached to tube (or small hose) entering water to depth of one meter or:

   b) Device can be clamped to piling, etc., or otherwise anchored to bottom in shallow water

   c) Structure should be likely to survive local effects of a tsunami

   d) Site must be accessible within one-half hour of usual location of observer/support personnel.

   e) Support personnel must be available who:
      1. Will maintain device in secure location
      2. Will be available or have good backup person, with one hour notice
      3. Are physically and mentally able to deploy and retrieve the device in an actual tsunami situation.

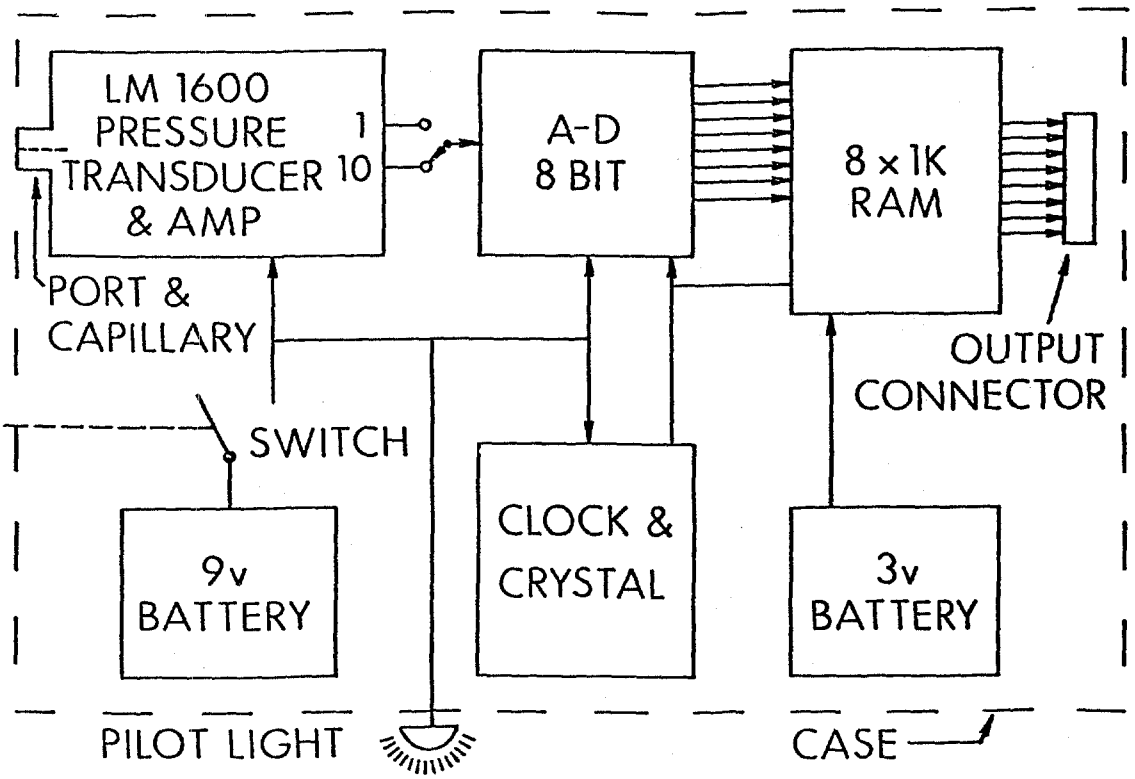

FIG 1 - BLOCK DIAGRAM, SOLID STATE GAGE

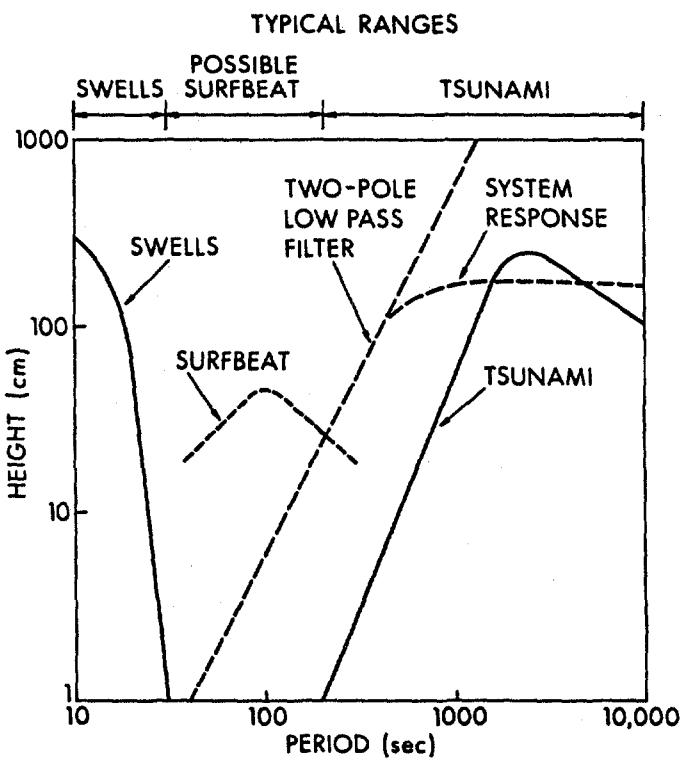

WAVE SPECTRA (VAN DORN, 1965) AND SYSTEM RESPONSE

FIG 2

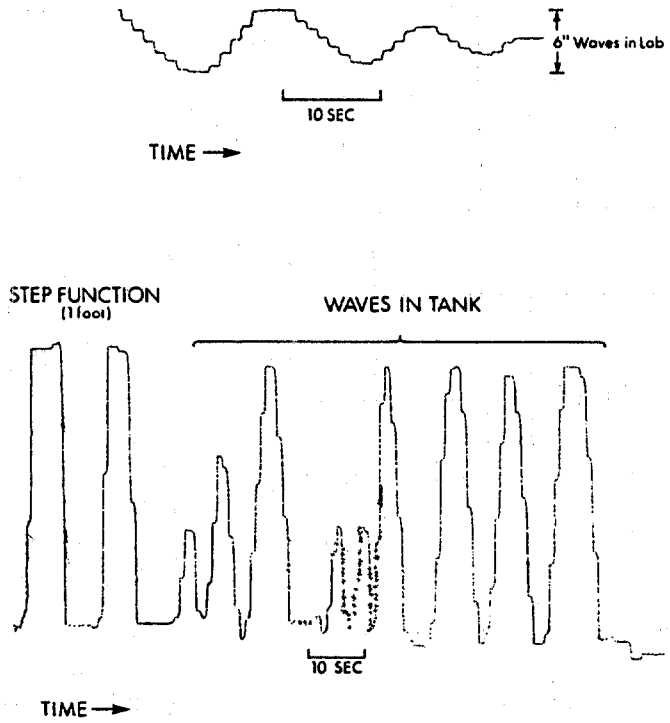

FIG 3 - LAB TESTS

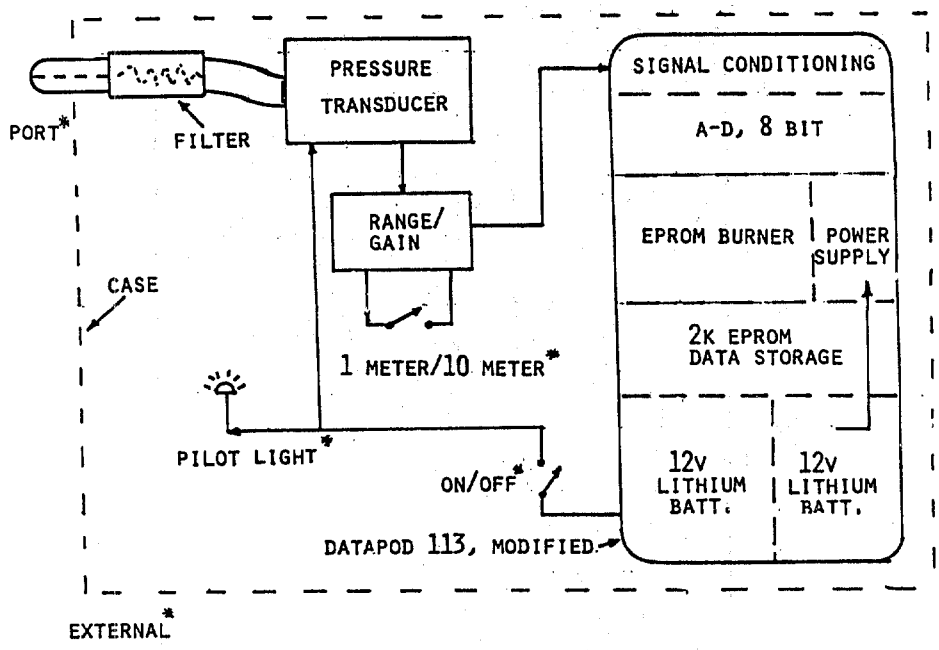

FIG 4 - FINAL DEVELOPMENT

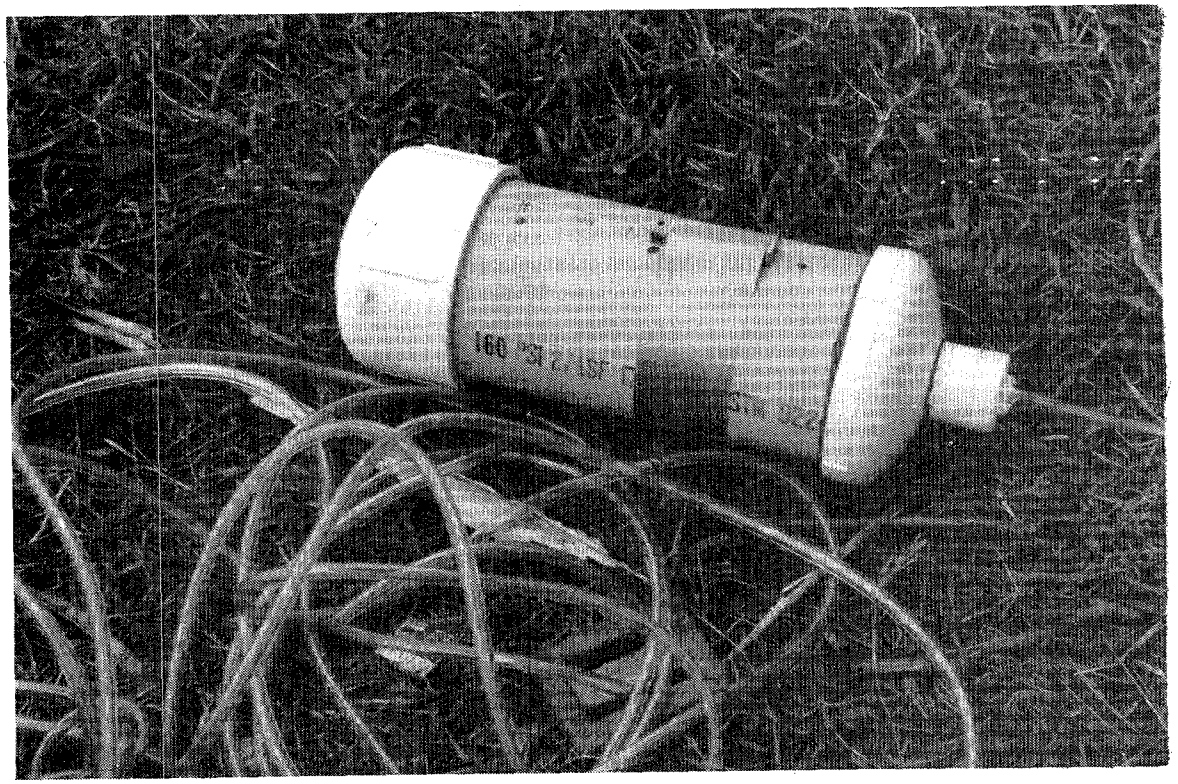

FIG 5 - NEW GAGE, UNDER TEST

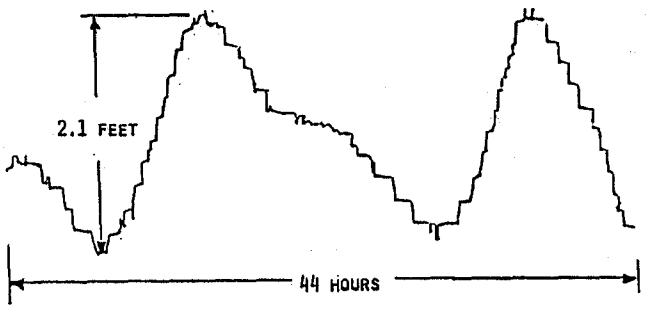

A - ANALOG PLOT FROM D-A CONVERTER

TIDE CYCLE - HAWAII

05	04	05	05	05	05	05	05
05	05	05	05	05	05	05	06
06	05	06	06	06	06	06	06
06	06	06	06	06	06	07	06
06	07	07	07	07	07	07	07
07	07	07	07	07	08	08	08
08	08	08	08	08	08	08	08
08	08	08	08	08	09	08	09
09	09	09	09	09	09	09	09
09	09	09	09	09	10	09	10
09	10	10	10	10	10	10	10
10	10	10	10	10	10	10	10
10	10	10	10	10	10	10	10
10	10	11	10	10	10	10	10
10	10	10	10	11	10	10	10
10	10	10	10	11	11	11	11
11	11	11	11	11	11	10	11
10	10	10	11	10	11	10	11
10	11	10	11	10	10	10	10
10	10	10	10	10	10	10	10

B - DIGITAL DATA (SAMPLE)

FIG 6 - DIGITAL GAGE
ON 10M RANGE, TIDE CYCLE

ACTIVITY OF TSUNAMIGENIC EARTHQUAKES AROUND THE PACIFIC

Kumizi Iida

Aichi Institute of Technology, Toyota, Japan

ABSTRACT

The activity of tsunamigenic earthquakes around the Pacific is investigated from 1900 to 1983. The frequency distribution of these earthquakes is examined in different area. The percentage of tsunami occurrence related to earthquake magnitude is different according to the area. Shallow submarine earthquakes having magnitude greater than 7.3 occurring in the sea adjacent to Japan are always accompanied by tsunami, while the tsunami occurrence in the earthquake magnitude over 8.0 is obtained in hundred percent in and near South America.

The frequency-height relation of tsunami at certain area can be expressed by

$$N(H)dH=kH^{-m}dH$$

or $$\log N'=c-m\log H, \qquad N'=\sum_{N} N(H)$$

here N(H)dH indicates the frequencies of tsunamis whose maximum heights are from H through H+dH; m, k and c are constants. The values of m representing tsunamicity are estimated at from about 0.7 to 2.1 for the tsunamis in Japan, New Guinea-Solomon and South America.

There seems to have a tendency for some regularities of the occurrences of large tsunamigenic earthquakes in South America where the locations of their epicenters successively migrated from north to south.

INTRODUCTION

Areas along the boundaries of the Pacific are known to be the most seismically active regions in the world, but there are many dissimilarities in areas of seismic activity which could potentially generate tsunamis. It is, therefore considered to be regional differences in tsunami activity. The present paper covers an investigation of all tsunamigenic earthquakes and tsunamis during the 84-year period from 1900 to 1983.

In consideration of the activity of these earthquakes and tsunamis around the Pacific, the frequency distribution of these earthquake occurrences is obtained for different regions. The tsunami activity is also investigated from a relation of tsunami height frequency which is especially taken into consideration of active regions such as Japan, South America, New Guinea and Solomon. Further, the relation between the tsunami-occurrence percentage and earthquake magnitude and the relation to focal depth are obtained from tsunami data in Japan and Chile; respectively.

As previously reported (Iida, 1983), it was found that there are some regions in Japan and Chile showing time regularities of destructive earthquake occurrences accompanied by tsunamis. The investigation of regularitis of large tsunamigenic earthquakes associated with their activities is also conducted for regions in South America related to the structure of island arcs and trenches where large earthquakes generate large tsunamis.

TSUNAMIGENIC EARTHQUAKE ACTIVITY

The earthquakes accompanied by tsunamis that occurred in the Pacific are investigated during the 84-year period from 1900 to 1983. The 385 tsunamis which were observed or recorded in the Pacific during this period are classified according to their occurrence region as given in Table 1, in which

TABLE 1 TSUNAMI ACTIVITY AROUND THE PACIFIC OCEAN

Region	Tsunami generation number	Percent
New Zealand-Kermadec-Tonga-Fiji-Samoa-New Caledonia-New Hebrides	36	9.4
New Britain-New Guinea-Solomon	61	15.8
Celebes-Java-Sumatora	22	5.7
Palau-Philippine	26	6.8
Japan-Taiwan	112	29.1
Kuril-Kamchatka	34	8.8
Aleutian-Alaska	22	5.7
Canada-U.S.A.	5	1.3
Mexico-Guatemala-Panama	24	6.2
Colombia-Peru-Chile	36	9.4
Hawaii	7	1.8
Total	385	100.0

tsunami region is divided into eleven and their frequency distributions are shown in Fig.1. The most active tsunami region is that of Japan-Taiwan where 29.1 percent of the total Pacific tsunamis were generated. Second active tsunami region is that of New Britain-New Guinea-Solomon where 15.8 percent tsunamis were generated. The tsunami active region following to these regions is those of Colombia-Peru-Chile and New Zealand-Kermadec-Tonga-Fiji-Samoa-New Caledonia-New Hebrides. The tsunami active region is related to the structure of island arcs and trenches, as shown in Fig.1 where large earthquakes frequently generate large tsunamis.

About 19 percent of the total Pacific tsunamis of 385 caused casualities and affected mainly the areas near their sources and about 5 percent of tsunamis caused widspread disaster even at places far from their sources.

Relating to the most active tsunami region, Japan and its neighboring countries are investigated during the 1300 year period from 684 to 1983. as shown in Fig.2, in which the epicenters of tsunamigenic earthquakes are plotted with circles whose size is related to earthquake magnitude. The most active region may be seen near the Pacific coast in Japan. A geographic distribution of tsunamigenic earthquakes in the Pacific Ocean is shown in Fig. 3, in which all the tsunamis reached or affected Japan and its vicinity are included. Tsunamis which caused some damage in Japan are found to be generated in the regions of South America, Kuril, Kamchatka, Aleutian and Alaska. The percentage of tsunamis propaged from South America to Japan is 25 percent in the range of earthquake magnitude from 7.9 to 8.1, and tsunamis generated by shallow submarine earthquakes having magnitudes greater than 8.3 are always propagated from South America to Japan, as shown by the broken line in Fig.5.

TSUNAMI OCCURRENCE PERCENTAGE AND ITS RELATION TO FOCAL DEPTH

The magnitude and the focal depth of an earthquake play an important role in the occurrence of a tsunami. Under these considerations, it is necessary to obtain a general relation between the magnitude and the focal depth of an earthquake accompanied by a tsunami in Japan and Chile. Fig.4 graphically shows the relation between these factors, where earthquakes occurring off the coast accompanied by tsunamis and those not accompanied by tsunamis are depicted by circles by filled-in circles and plain circles respectively. From Fig.4 a, b it may be noticed that there is an approximate linear boundary between the earthquakes accompanied by tsunamis and those not accompanied by tsunamis. This means that there is a limiting magnitude for earthquakes under which tsunamis do not occur. The earthquake magnitude M may be expressed by a relation which is linear with respect to the focal depth H. Thus the limit may be generally expressed by

$$M = 5.75 + 0.015H \quad \text{for Chile,}$$
$$M = 5.80 + 0.010H \quad \text{for Japan,}$$

and the limit for moderate or disastrous tsunamis also may be determined by

$$M = 7.90 + 0.0071H \quad \text{for Chile,}$$
$$M = 7.41 + 0.0086H \quad \text{for Japan,}$$

as shown by the broken line in Fig.4 a, b. Thus it may be concluded that the magnitude of earthquakes which might have produced tsunami is generally larger than 5.8 in the region of Chile and Japan, respectively. When the earthquake magnitude is greater than 7.4 and 7.9 moderate or disasterous tsunami occurs in the region of Japan and Chile, respectively, as shown in Fig.4a,b. Shallow submarine earthquake having a magnitude greater than 7.3 occurring in the sea adjacent to Japan, as shown in Fig.5 is always accompanied by tsunami while the tsunami occurrence in the earthquake magnitude over 8 in Chile is obtained in 100 percent. Here, tsunami materials of Iida (1984) and Lockridge (1985) are used.

TSUNAMI HEIGHT FREQUENCY AND ITS RELATION TO EARTHQUAKE MAGNITUDE

130 tsunamis were observed in Japan from 1900 to 1984. 72 percent of them were generated by earthquakes occurring near Japan. Fig.6a shows the frequency distribution of maximum amplitude or height of tsunamis in the whole of Japan and the Sanriku area. The abscissa and ordinate are on a logarithmic scale. The linear relation between them is denoted by

$$N(H)dH = kH^{-m}dH,$$

or

$$\log N' = c - m\log H, \qquad N' = \sum_{N} N(H)$$

where N(H)dH and N' indicate those frequencies of tsunamis whose maximum amplitudes or heights are from H through H + dH and larger than H, respectively. k, m and c are constants.

This relationship was already found for the frequency distribution of tsunamis in Japan and Hawaii by Iida(1965), which was similar to the formula of Ishimoto and Iida (1939) obtained by the frequency distribution of the maximum amplitude of earthquake waves at a certain station. This relationship was also found for Tofino in Canada by Wigen (1977) and for Miyako in Japan by Okada and Tada (1983). The parameter m is estimated as 0.74 for the whole of Japan and 0.71 for the Sanriku district, respectively.

Fig.6b shows the frequency distribution of maximum height of tsunamis in the Peru-Chile and the New Britain-New Guinea-Solomon region, respectively. The parameter m is estimated as 0.88 for the former region and 1.15 for the latter region, respectively. Thus, the values of m representing tsunamicity are estimated as about 0.7 to 2.1 for the tsunamis in various regions.

Since N represents the number of events for a 84-year period, the maximum wave height of a once-in-a-century tsunami at various regions above mentioned can be caluculated. The values of tsunami height thus obtained are given in Table 2. From this table we can see that large tsunami might attack at some region once per century.

TABLE 2. PARAMETER M AND CENTURY TSUNAMI HEIGHT

Region	m	c	Century tsunami height(m)
Whole Japan	0.74	2.86	65.0
Sanriku district	0.71	2.33	24.7
Peru-Chile	0.88	3.17	47.3
New Britain-New Guinea-Solomon	1.15	4.00	34.9
Tofino (by Wigen)	1.04	2.40	2.7
Miyako (by Okada)	2.1	2.76	5.0

Fig.7 shows the relationship between the maximum height of tsunamis and the earthquake magnitude in Japan from 1900 to 1983. From this figure we find that in general the greater the magnitude, M of the earthquake, the greater the height, H of the tsunami and thus the relation has been found to be

$$\log H = 1.73M-10.71;$$

in which the numerical values are determined by the least squares method. We may estimate the maximum height of tsunamis in Japan as about ten meters for the earthquake magnitude of 7.9.

OCCURRENCES OF LARGE TSUNAMIGENIC EARTHQUAKES IN SOUTH AMERICA

As already discussed (Iida 983), regularities of occurrence of large tsunamigenic earthquakes in time and space were found for regions related to the structure of island arcs and trenches. These regions are the Tokai-Nankai and the Sanriku district in Japan and the Valparaiso area to the Valdivia region in Chile. This papers to the occurrence of large earthquakes and tsunamis in South America. Fig.8 shows the epicenter distribution of tsunamigenic earthquakes with a magnitude greater than 7.6 and seven geographic regions of earthquake districts, each of which has 4-6 degrees in latitude. We designate these earthquake districts as Trujillo-Lima (8°s-13°s), Pisco-Arica (13°s-18.5°s),, Pisagua-Tocopilla-Antofagasta (18.5°s-25.5°s), Taltal-Caldera-La Serena (25.5°s-29.5°s), Coquinbo-Valparaiso-San Antonio (29.5°s-33.5°s), Constitucion-Concepcion-Lebu (33.5°s-37.5°s), Saavedra-Valdivia-Puerto Aisen (37.5°s-45°s). The large earthquakes occurred in these seven regions are arranged in time and space, as shown in Fig.9, from which we may find six earthquake sequences:

(1) The earthquakes of 1562 (Valparaiso), 1570 (Concepcion), 1575 (Valdivia). An arrangement was not possible for lack of historical data before 1562.

(2) The earthquakes of 1586 (Lima), 1604 (Arica), 1615 (Tocopilla), 1647 (Valparaiso), 1657 (Concepcion).
(3) The earthquakes of 1678 (Lima), 1687 (Tocopilla), 1705 (Caldera), 1715 (Caldera), 1730 (Valparaiso), 1737 (Valdivia), 1751 (Concepcion).
(4) The earthquakes of 1746 (Lima), 1765 (Tocopilla), 1819 (Caldera), 1822 (Valparaiso), 1835 (Concepcion), 1837 (Valdivia).
(5) The earthquakes of 1847 (Lima), 1868 (Arica), 1859 (Caldera), 1877 (Tocopilla), 1906 (Valparaiso), 1928 (Concepcion), 1960 (Valdivia) and other branch earthquake sequences of 1918 and 1922 (Caldera), 1943 (Valparaiso).
(6) The earthquakes of 1940 (Lima), 1942 (Arica), 1966 (Caldera), 1985 (Valparaiso).

THe time period taken for each earthquake sequence is found to be 81 years from 1586 to 1657, 73 years from 1678 to 1751, 91 years from 1746 to 1837, 113 years from 1847 to 1960, respectively. Average value of these periods is about 89 years. Thus, the occurrence of these sequential large tsunamigenic earthquaks appears to have migrated succesively southward from Peru to Chile with the 89-year period.

The time intervals between large earthquakes occurred in adjacent earthquake districts in each earthquake sequence are in the ranges of 2 to 32 years. Therefore, we may predict an earthquake occurrence in the Concepcion or Valdivia region from the earthquake occurrence in the sixth earthquake sequence originated in 1940 in the Lima region. The time intervals between earthquake occurrences in the Lima and Concepcion region in Fig.9 are estimated as 81, 73, 89, 81 years for each earthquake sequence, respectively, and mean interval of these values is 81 years. Then an earthquake occurrence in the Concepcion region will be in 2021. If we take time intervals between the earthquake occurrences in the Valparaiso to the Concepcion region, an earthquake ocurrences in the Concepcion will be in 1993-2007. In the some way, if we will consider the mean interval of earthquake sequences and time intervals between earthquake occurrences in the Valparaiso and Valdivia region, an earthquake occurrence in the Valdivia region will be estimated as 2029 or 1998-2002. These considerations are made under the assumption of the same process of earthquake occurrence in these regions.

The time intervals between earthquake sequences are found in the earthquake occurrence originated in the Lima region in the range of 68 years to 101 years, where the intervals are 92 years from 1586 to 1678, 68 years from 1678 to 1746, 101 years from 1746 to 1847, 83 years from 1847 to 1940, and 26 years from 1940 to 1966. The last time interval seems to be too short compared with other intervals. Therefore, it is difficult to assume as an earthquake sequence originated in the Lima region similar to other earthquake sequence in the past.

CONCLUDING REMARKS

The activity of tsunamigenic earthquakes around the Pacific was investigated for the period from 1900 to 1984 and a compilation was made of those earthquakes and tsunamis which caused damage in coastal areas. During this period the number of tsunamis accompanying submarine earthquakes totaled 385. The most active region is that of Japan-Taiwan where 29.1 percent of the total Pacific tsunamis were generated. It was found that the magnitude of earthquakes accompanied by tsunamis is larger than 5.8 in the region of Chile and Japan, and that shallow submarine earthquake with a magnitude greater than 7.3 in Japan and 8.0 in Chile, respectively, is always accompanied by tsunamis.

Tsunami height frequency and maximum wave height of a once-in-a-century tsunami at some regions are also investigated. It is necessary to extend this investigation to other regions around the Pacific except the regions in Table 2, in which tsunamicity parameters and a century tsunami height

are given. Some regularities of occurrence of large tsunamigenic earthquakes in time and space were found in South America. These earthquakes appear to have migrated successively southward from Peru to Chile with an average time-interval of 89 years. The time interval of repeated occurrence of earthquake sequences appears to be in the range of 68 to 101 years. If the same process of these earthquake occurrence around the Pacific is assumed, from the present results the possibility is suggested of future large tsunamigenic earthquakes in the Concepcion and Valdivia region.

REFERENCES

Iida,K., Behavier of Tsunami in the Nearshore, U.S.-Japan Cooperative Scientific Research Seminars on Tsunami Run-up, Sapporo and Tokyo,1965.

Iida,K., Some Remarks on the Occurrence of Tsunamigenic Earthquakes around the Pacific, Tsunamis, Their Science and Engineering, edited by K.Iida and T.Iwasaki, Terrapub, Tokyo, 61-76, 1983.

Iida,K., Catalog of Tsunamis in Japan and its Neighboring Countries, special report of Aichi Institute of Technology, Toyota, 1984.

Ishimoto,M., and K.Iida, Observations sur les seismes enregistres par le microseismographe construit dernierement(1), Bull. Earthq. Res, Inst., Tokyo Univ., 17, 443-478, 1939 (in Japanese).

Lockridge,P.A., Tsunamis in Peru-Chile, World Data Center A for Solid Earth Geophysics, U.S. Department of Commerce., Report SE-39, 1985.

Okada,M. and M.Tada, Historical Study of Tsunamis at Miyako, Japan,Tsunamis, Their Science and Engineering. edited by K.Iida and T.Iwasaki, Terrapub, Tokyo, 121-130, 1983.

Wigen,S.O., Tsunami threat to port Alberni, Prepared for consulting engineers Allan M.McCrae, Victoria, B.C., and Reid Crowther and Partmers Ltd., Vancouver, B.C.,1977.

Wigen,S.O., Historical Study of Tsunamis at Tofino, Canada, Tsunamis, Their Science and Engineering, edited by K.Iida and T.Iwasaki, Terrapub, Tokyo, 105-119, 1983.

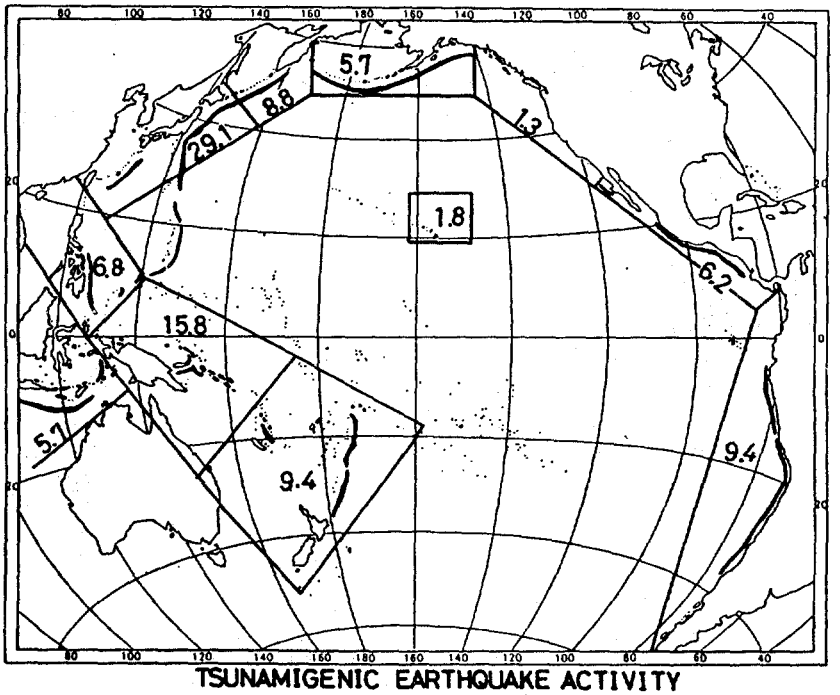

Fig.1. Regional tsunami activities in the Pacific Ocean expressed in percent Thick lines denote the ocean trenches.

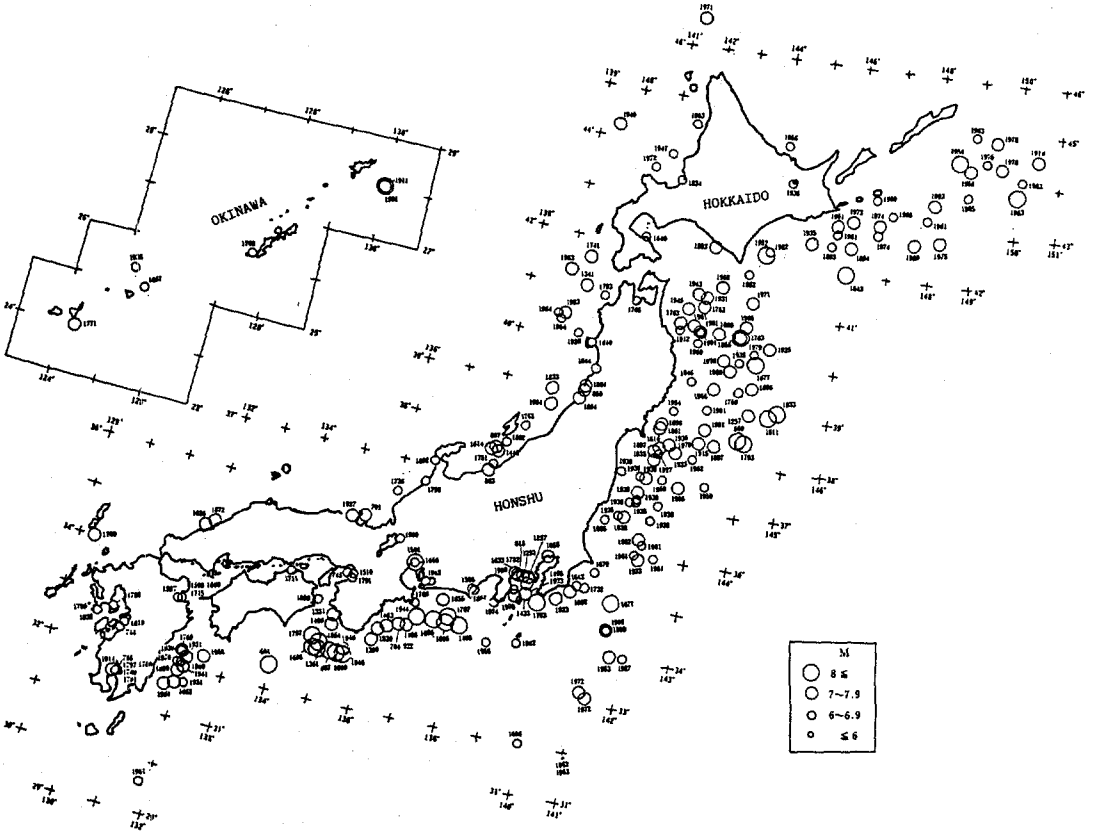

Fig.2. Geographic distribution of epicenters of tsunamigenic earthquakes occurred in and near Japan. The epicenters are plotted with circles whose size is related to earthquake magnitude.

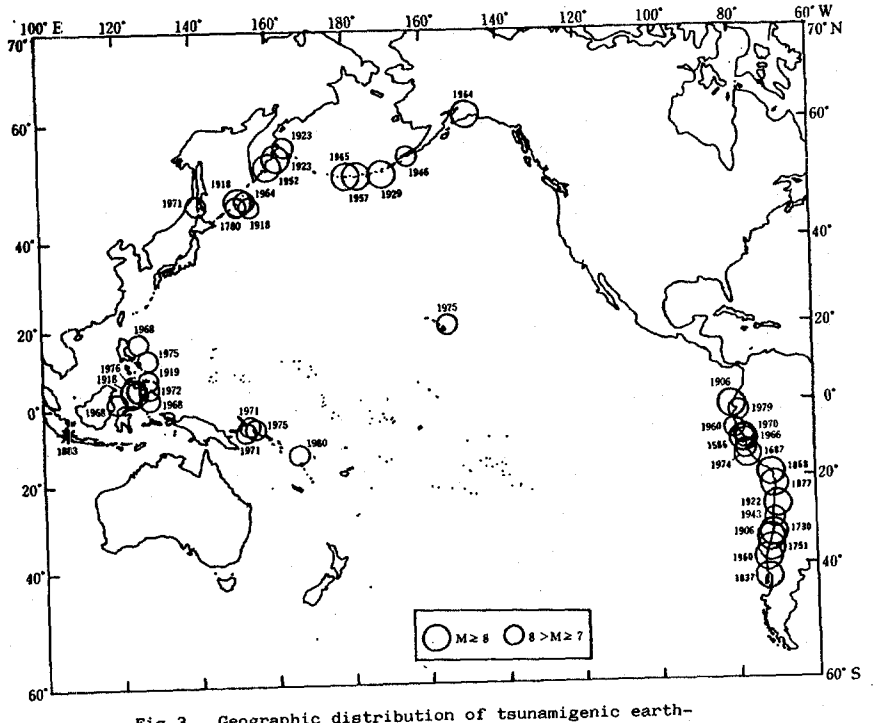

Fig.3. Geographic distribution of tsunamigenic earthquakes in the Pacific Ocean, whose tsunamis reached and affected Japan. Gothic type year shows tsunami which caused some damage in Japan and its vicinity.

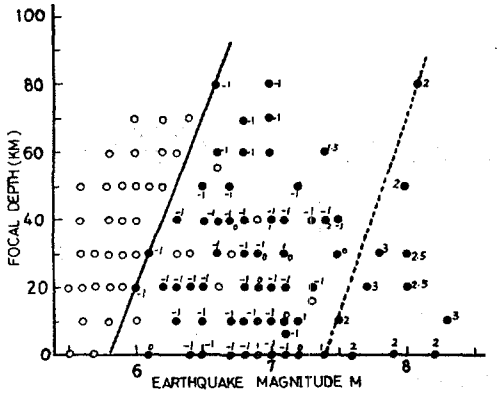

Fig.4a. Relationship between magnitude and focal depth of tsunamigenic earthquakes in Japan.

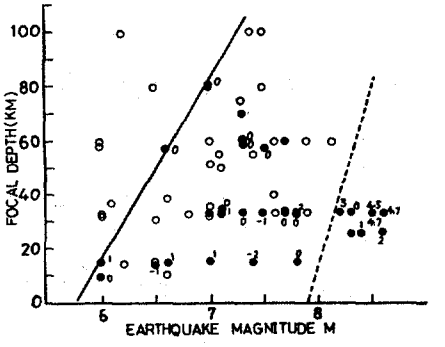

Fig.4b. Relationship between magnitude and focal depth of tsunamigenic earthquakes in Chile.

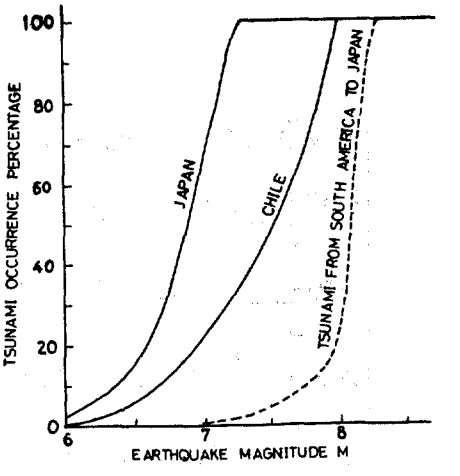

Fig.5. Percentage of tsunami occurrence related to earthquake magnitude in Chile and Japan.

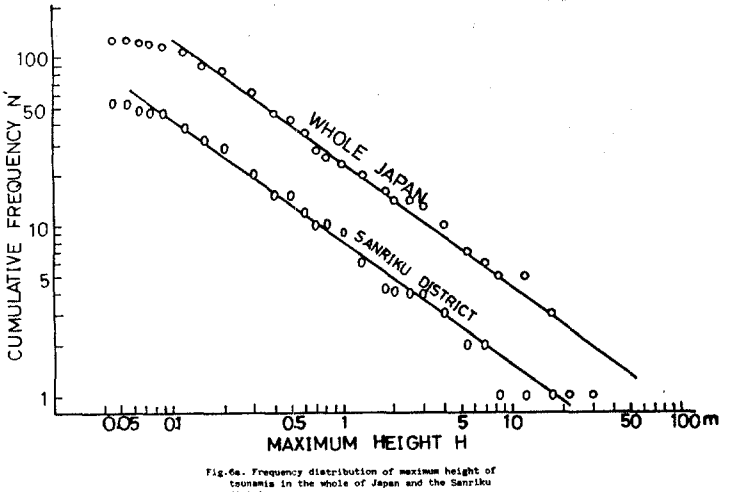

Fig.6a. Frequency distribution of maximum height of tsunamis in the whole of Japan and the Sanriku district.

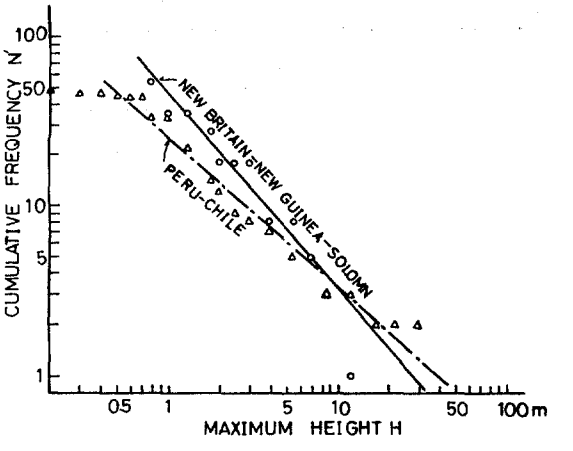

Fig.6b. Frequency distribution of maximum height of tsunamis in the Peru-Chile and the New Britain-New Guinea-Solomon region.

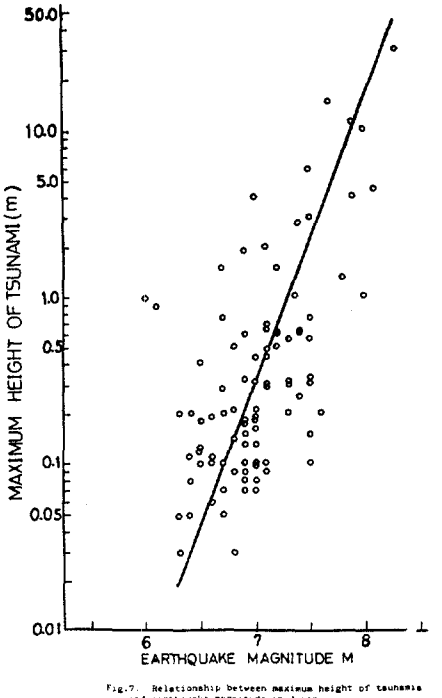

Fig.7. Relationship between maximum height of tsunamis and earthquake magnitude in Japan.

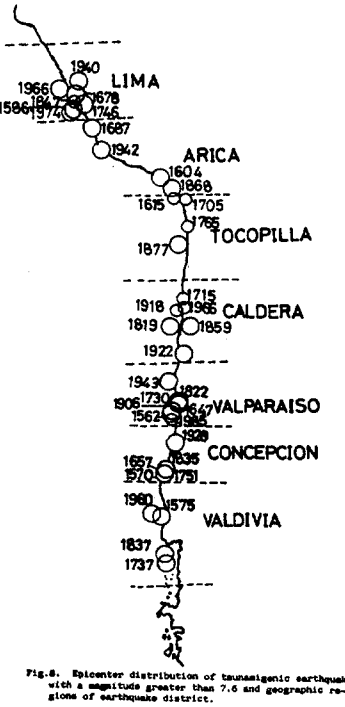

Fig.8. Epicenter distribution of tsunamigenic earthquakes with a magnitude greater than 7.6 and geographic regions of earthquake district.

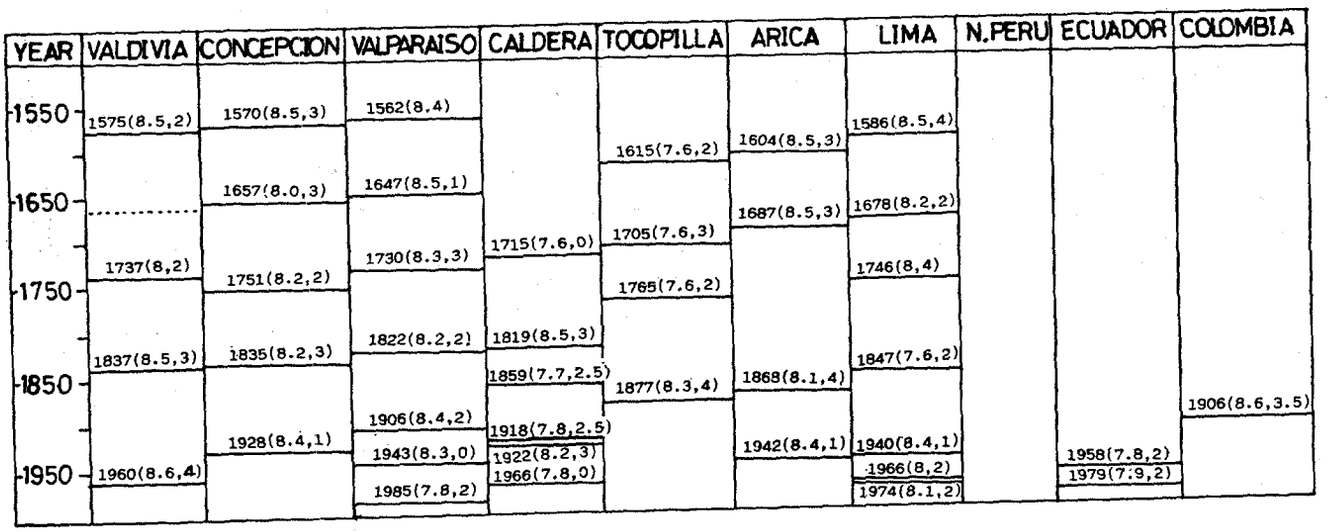

Fig.9 Sequential occurrences of great tsunamigenic earthquakes in the earthquake district in South America. The 600 km segment along the coast from Ecuador to North Peru is a region of low seismic activity region since historic times. Numeral indicates earthquake occurrence year and bracket numeral indicates earthquake magnitude and tsunami magnitude.

APPLICATION FOR MEMBERSHIP

THE TSUNAMI SOCIETY
P.O. Box 8523
Honolulu, Hawaii 96815, USA

I desire admission into the Tsunami Society as: (Check appropriate box.)

☐ Student ☐ Member ☐ Institutional Member

Name _____ Signature _____

Address _____ Phone No. _____

_____

Zip Code _____ Country _____

Employed by _____

Address _____

Title of your position _____

FEE: Student $5.00 Member $25.00 Institution $100.00

Fee includes a subscription to the society journal: SCIENCE OF TSUNAMI HAZARDS.

Send dues for one year with application. Membership shall date from 1 January of the year in which the applicant joins. Membership of an applicant applying on or after October 1 will begin with 1 January of the succeeding calendar year and his first dues payment will be applied to that year.